CHEMISTRY
A EUROPEAN JOURNAL

DOI: 10.1002/chem.200700013

# Charge Decomposition Analysis of the Electron Localizability Indicator: A Bridge between the Orbital and Direct Space Representation of the Chemical Bond

**Frank R. Wagner,* Viktor Bezugly, Miroslav Kohout, and Yuri Grin[a]**

**Abstract:** The novel functional electron localizability indicator is a useful tool for investigating chemical bonding in molecules and solids. In contrast to the traditional electron localization function (ELF), the electron localizability indicator is shown to be exactly decomposable into partial orbital contributions even though it displays at the single-determinantal level of theory the same topology as the ELF. This approach is generally valid for molecules and crystals at either the single-determinantal or the explicitly correlated level of theory. The advantages of the new approach are illustrated for the argon atom, homonuclear dimers $N_2$ and $F_2$, unsaturated hydrocarbons $C_2H_4$ and $C_6H_6$, and the transition-metal-containing molecules $Sc_2^{2+}$ and $TiF_4$.

**Keywords:** bond theory · chemical bonds · electron localizability indicator · ELF (electron localization function) · localized orbitals

## Introduction

The electron localization function (ELF) originally defined by Becke and Edgecombe[1] for a Hartree–Fock (HF) wavefunction has proven to be a valuable quantum mechanical tool for bonding analysis in position space. One drawback to its use has been the unknown physical content of this function as it has been defined in axiomatic manner employing an arbitrary division of the position-dependent, spherically averaged conditional pair probability density by that of a reference model system, namely, the free electron gas. Another problem, in fact connected with the first one, is the difficulty of uniquely defining the ELF at a correlated level of theory. Recently, a functional termed the electron localizability indicator[2] (ELI) was derived directly from the electron-pair density without any reference system using a novel scheme that can be generalized to yield the restricted populations approach.[3] The ELI was initially designed to depict the position-dependent fraction of a same-spin electron pair per fixed, sufficiently small charge enclosed in compact regions (micro-cells) in space and was therefore denoted as ELI-q. In the meantime another variant of the ELI, named ELI-D, which depicts the average number of electrons per fixed fraction of a same-spin electron pair, was derived and applied in momentum space.[4,5] Being quite generally defined for the correlated pair density of a time-dependent many-body wavefunction for the case of a time-independent single-determinantal wavefunction, the ELI-D formally simplifies to the inverse of the relevant kernel of the ELF. For this reason it has an identical topology to the ELF. However, the ELI-D should not be considered as a generalization of the ELF formula, but a separate though related quantity that represents one possible physical interpretation of the ELF kernel at a correlated level of theory. Other physical interpretations of the ELF kernel may lead to different expressions at a correlated level of theory.[6] Adopting the ELI-D interpretation of the ELF kernel gives rise to both 1) new concepts on how to work with it as well as 2) strict limitations of applicability beyond which the physical content will be lost.

In this contribution we will elaborate the method for orbital decomposition of the ELI-D in direct space. The orbital concept is widely used in chemistry and physics and orbital decomposition of the ELI-D will enable a bridge to be built between the Hilbert and direct space representations of the chemical bond.

[a] Dr. F. R. Wagner, Dr. V. Bezugly, Dr. M. Kohout, Prof. Dr. Yu. Grin
Max-Planck-Institut für Chemische Physik fester Stoffe
Nöthnitzer Straße 40, 01187 Dresden (Germany)
Fax: (+49) 351-4646-4002
E-mail: wagner@cpfs.mpg.de

## Charge decomposition of the ELI-D

In the following, the basic theory underlying the definition of the ELI-D is briefly reviewed in order to familiarize the

reader with its basic concepts. This will lead to the decisive equation [Eq. (11)] with the mathematically exact orbital-resolved definition of the ELI-D applicable to molecules and solids at both the single-determinantal and the explicitly correlated level of theory. For the detailed derivation, a reference to the original work is given at each necessary place. In a subsequent step we discuss why within the framework of the ELF and the spin-pair composition function such a procedure would be incompatible with the basic ideas behind them (see Appendix).

Previously, the electron localizability indicator ELI-q,[2] a functional in position and in momentum space,[4,5] was derived directly from the same-spin pair density such that it is defined at a wavefunction-based fully correlated level of theory as well.[6] The method used can be generalized to yield the so-called restricted populations approach.[3] Within this method two different position-dependent properties, generally called the control and the sampling properties, are interconnected. The control property forms the basis for partitioning of space into compact, mutually exclusive and space-filling micro-cells with variable volumes. The volumes of the micro-cells can be considered a response of the system to the so-called $\omega$-restriction: the scalar control quantity $\omega$, that is, the integrated value of the position-dependent control property, is restricted to have a fixed value for all micro-cells. The sampling property is then integrated within each of these micro-cells giving rise to a discrete distribution of the sampling quantity. The electron density $\rho(\boldsymbol{r})$ and the same-spin pair density $\rho_2^{\sigma\sigma}(\boldsymbol{r}_1,\boldsymbol{r}_2)$ are the two properties interconnected by the ELI in position space. The two different aspects of the ELI arise from the freedom to exchange the control and sampling property without changing the basic content of the ELI functional. Thus, the control quantity can be either the charge $q$ or the number of same-spin electron pairs $D^{\sigma\sigma}$. The sampling quantity is then the other quantity. This forms the basis of the discrete distribution $\Upsilon_\omega^s$, where the subscript denotes the control quantity $\omega$ used for the restriction and the superscript denotes the spin of the sampling property. The two aspects of the ELI, namely ELI-q $\Upsilon_q^\sigma$ and ELI-D $\Upsilon_D^\sigma$, represent discrete distributions in real (i.e., momentum) space whose local values are proportional to the respective values of the sampling quantity (see below).

For the charge decomposition analysis the ELI-D is the decisive functional. It has already been explicitly derived in momentum space by Kohout et al.[4] Since the principal equations in position space are in a very simple 1:1 fashion related to those in momentum space (i.e., a change of the space coordinate from momentum $\boldsymbol{p}$ to position $\boldsymbol{r}$ and momentum density $\pi(\boldsymbol{p})$ corresponds to electron density $\rho(\boldsymbol{r})$), there is no need to explicitly repeat the whole derivation for the ELI-D in position space.

The ELI-D is obtained by imposing the restriction of an infinitesimally small fraction of a same-spin electron pair $D^{\sigma\sigma}$ in each micro-cell. This gives rise to a discrete, quasi-continuous distribution of positions $\{\boldsymbol{a}_1, \boldsymbol{a}_2, \ldots, \boldsymbol{a}_M\}$ at which such micro-cells are centered. In each micro-cell the (variable) charge $Q_i$ is determined (not to be intermixed with the fixed charge $q$ used in $q$-restricted partitioning in the ELI-q), which yields the corresponding discrete distribution of charges $\{Q_1, Q_2, \ldots, Q_M\}$. The ELI-D is a discrete distribution of values $\{\Upsilon_D^\sigma(\boldsymbol{a}_1), \Upsilon_D^\sigma(\boldsymbol{a}_2), \ldots, \Upsilon_D^\sigma(\boldsymbol{a}_M)\}$ proportional to the corresponding charges $Q_i$.

Of course, the charge $Q_i$ and the number of same-spin electron pairs $D^{\sigma\sigma}$ are given as the respective integral of the electron density $\rho(\boldsymbol{r})$ and the same-spin pair density $\rho_2^{\sigma\sigma}(\boldsymbol{r}_1,\boldsymbol{r}_2)$ over the given micro-cell volume. Fortunately these integrals need not be calculated explicitly.[2] Instead, in the actual calculations an approximation is used to determine the integrals: for a very small micro-cell volume $V_i$ the σ spin charge $Q_i^\sigma$ can be approximated by Equation (1).

$$Q_\mathrm{i}^\sigma \approx \rho_\sigma(\boldsymbol{a}_i)V_i \tag{1}$$

Furthermore, the number of same-spin pairs $D^{\sigma\sigma}$ in $V_i$ is approximated[2] using the Taylor expansion to yield Equation (2)

$$D^{\sigma\sigma} \approx \frac{1}{12}V_i^{8/3}g(\boldsymbol{a}_i) \tag{2}$$

with the Fermi hole curvature[6,7] $g(\boldsymbol{a}_i)$ at position $\boldsymbol{a}_i$. From Equation (2) the expression for volume $V_i$ is obtained [Eq. (3); $D^{\sigma\sigma}$ is the control quantity, i.e., it has a fixed value].

$$V_i \approx \left(\frac{12D^{\sigma\sigma}}{g(\boldsymbol{a}_i)}\right)^{3/8} \tag{3}$$

Inserting Equation (3) into Equation (1) yields Equation (4).

$$Q_\mathrm{i}^\sigma \approx (D^{\sigma\sigma})^{3/8}\rho(\boldsymbol{a}_i)\left(\frac{12}{g(\boldsymbol{a}_i)}\right)^{3/8} \tag{4}$$

ELI-D is defined in such a way as to give Equation (5).

$$Q_\mathrm{i}^\sigma = (D^{\sigma\sigma})^{3/8}\Upsilon_D^\sigma(\boldsymbol{a}_i) \tag{5}$$

Since $D^{\sigma\sigma}$ is given a fixed value for all systems, the ELI-D is proportional to the charge $Q_i^\sigma$ within each micro-cell [Eq. (6)].

$$\Upsilon_D^\sigma(\boldsymbol{a}_i) = \frac{Q_\mathrm{i}^\sigma}{(D^{\sigma\sigma})^{3/8}} \approx \rho(\boldsymbol{a}_i)\frac{V_i}{(D^{\sigma\sigma})^{3/8}} = \rho(\boldsymbol{a}_i)\tilde{V}_\mathrm{D}(\boldsymbol{a}_i) \tag{6}$$

From the first equality the ELI-D can be seen to be proportional to the charge (average number of electrons) given by $Q_i^\sigma$ which is needed to form a fixed fraction $D^{\sigma\sigma}$ of a same-spin electron pair. The scaled volumes $\tilde{V}_D(\boldsymbol{a}_i)$ are termed the pair-volume distribution.

As already mentioned, the ELI-D represents a quasicontinuous distribution. For infinitesimally small values of the control quantity $D^{\sigma\sigma}$ this distribution will be so dense that

  

for convenience the discrete positions can be regarded as continuous [Eq. (7)] and $\Upsilon_D^\sigma(\boldsymbol{r})$ can be expressed as the product of the electron density with the pair-volume function $\tilde{V}_D(\boldsymbol{r})$ [Eq. (8)].

$$\Upsilon_D^\sigma(\boldsymbol{a}_i)|_{D\sigma\sigma\to 0} \to \Upsilon_D^\sigma(\boldsymbol{r}) \tag{7}$$

$$\Upsilon_D^\sigma(\boldsymbol{r}) = \rho(\boldsymbol{r})\tilde{V}_D(\boldsymbol{r}) = \rho(\boldsymbol{r})\left(\frac{12}{g(\boldsymbol{r})}\right)^{3/8} \tag{8}$$

For the sake of completeness we note that there is a non-trivial relation between the ELI-D and the ELI-q[3] [Eq. (9)].

$$\Upsilon_D^\sigma(\boldsymbol{r}) = \left(\frac{1}{\Upsilon_q^\sigma(\boldsymbol{r})}\right)^{3/8} \tag{9}$$

Note, within the framework of the restricted populations approach the electron density $\rho(\boldsymbol{r})$ itself can also be interpreted as a discrete quasi-continuous charge distribution [Eq. (10)] with the volumes $V(\boldsymbol{a}_i)$ of the micro-cells centered at $\boldsymbol{a}_i$ fixed at a constant value $V_{\text{const.}}$ throughout space. In other words, the charge density at each point is interpreted as the number of electrons per fixed volume. Furthermore, as the volumes are chosen to be non-overlapping and space-filling, the charge distribution fulfils the law of charge conservation: the sum over all $q(\boldsymbol{a}_i)$ gives the total number of electrons.

$$q(\boldsymbol{a}_i) \approx \rho(\boldsymbol{a}_i)V(\boldsymbol{a}_i) = \rho(\boldsymbol{a}_i)V_{\text{const.}} \tag{10}$$

The topological analysis of the electron density $\rho(\boldsymbol{r})$ for the definition of atoms-in-molecules was introduced by Bader.[8] To define the elements of chemical bonding in position space—bonds and lone pairs, atomic core shells and the valence shell—it is proposed that the topology of a different kind of charge distribution should be analyzed, namely the charges $Q_i^\sigma$ per fixed fraction $D^{\sigma\sigma}$ of the same-spin electron pair, that is, the ELI-D. Taking the point of view that the isotopological ELF is in a certain sense related to the time-independent HF approximation of the ELI, it has already proven its usefulness in many studies since 1990, the birth date of the ELF.[1] Beyond that, the use of the ELI-D now opens up the possibility of exactly decomposing the total ELI-D into additive positive contributions in the same way that the electron density can be decomposed [Eq. (11)].

$$\begin{aligned}\Upsilon_D^\sigma(\boldsymbol{r}) &= \sum_l^{\text{occ.}} \rho_{\sigma,l}(\boldsymbol{r})\left[\frac{12}{g(\boldsymbol{r})}\right]^{3/8} \\ &= \sum_l^{\text{occ.}} \rho_{\sigma,l}(\boldsymbol{r})\tilde{V}_D(\boldsymbol{r}) = \sum_l \Upsilon_{D,l}^\sigma(\boldsymbol{r})\end{aligned} \tag{11}$$

This makes possible the decomposition of the ELI-D into contributions $\rho_{\sigma,l}$ from, for example, 1) canonical or localized orbitals or orbital sets, 2) α and β spin channels (spin-polarized calculations), 3) natural orbitals (correlated wavefunctions), 4) (partial) **k**-summed energy bands (for solids), and 5) Wannier functions (for solids).

In this contribution we will restrict ourselves to the orbital decomposition of the ELI-D for molecules. In the following the orbital contributions $\Upsilon_{D,l}^\sigma$ to the total ELI-D will be denoted as the "partial ELI-D" (pELI-D) contributions.

The significance of the pELI-D contributions is clarified by the following: it monitors the portion of charge that a selected orbital contributes to the total charge contained in each micro-cell enclosing the same (fixed) fraction of a same-spin electron pair. The topology of the pELI-D contributions can be regarded as arising from the product of the orbital density and a position-dependent weighting factor, that is, the pair-volume function, which is inversely proportional to the Fermi hole curvature $g(\boldsymbol{r})^{3/8}$.

To show the usefulness of our definition of the pELI-D contributions we present in the Results section a few illustrative examples and analyses.

In view of the explicit derivation of the ELI-D from the electron-pair density, application of the ELI-D is strictly justified within wavefunction-based theories, that is, HF and post-HF methods such as the complete active space (CAS) and configuration interaction (CI) methods. Therefore, for all examples discussed below we applied the HF method. From a less puristic and more pragmatic point of view calculation of the ELI-D from Kohn–Sham orbitals within the framework of DFT can be justified only through the quality of the results. We therefore additionally calculated for all examples the ELI-D from the "Kohn–Sham determinantal wavefunction",[9] that is, the Slater determinant constructed from occupied Kohn–Sham orbitals. Besides some minor quantitative differences, the results of the HF and DFT calculations are found to be qualitatively the same for all but one example, namely $F_2$. For this molecule, which is known to be badly represented at the HF level, HF and DFT give slightly different ELI-D topologies for the bonding region. To make a decision as to the correct topology, a qualitatively better wavefunction from a CAS calculation was used which corroborated the DFT result. Although this finding cannot be easily generalized, it shows that the ELI-D calculated from Kohn–Sham orbitals should be considered to be at least on a similar level in terms of quality as the HF one. In order to decide on the correct topology in situations in which different topologies were given by the two methods, a definitively better wavefunction-based correlated calculation has to be used. In the examples given below, if not stated otherwise, the HF results are explicitly depicted and discussed.

## Methods

The electronic structure calculations at the HF level were performed with the MOLPRO program system[10] and the ones at the CAS level with the MOLCAS program system [11] using implemented all-electron valence triple-zeta basis sets with two sets of polarization functions (named cc-pvtz). The electronic structure calculations at the DFT level were performed with the ADF program system[12] at the generalized gra-

  

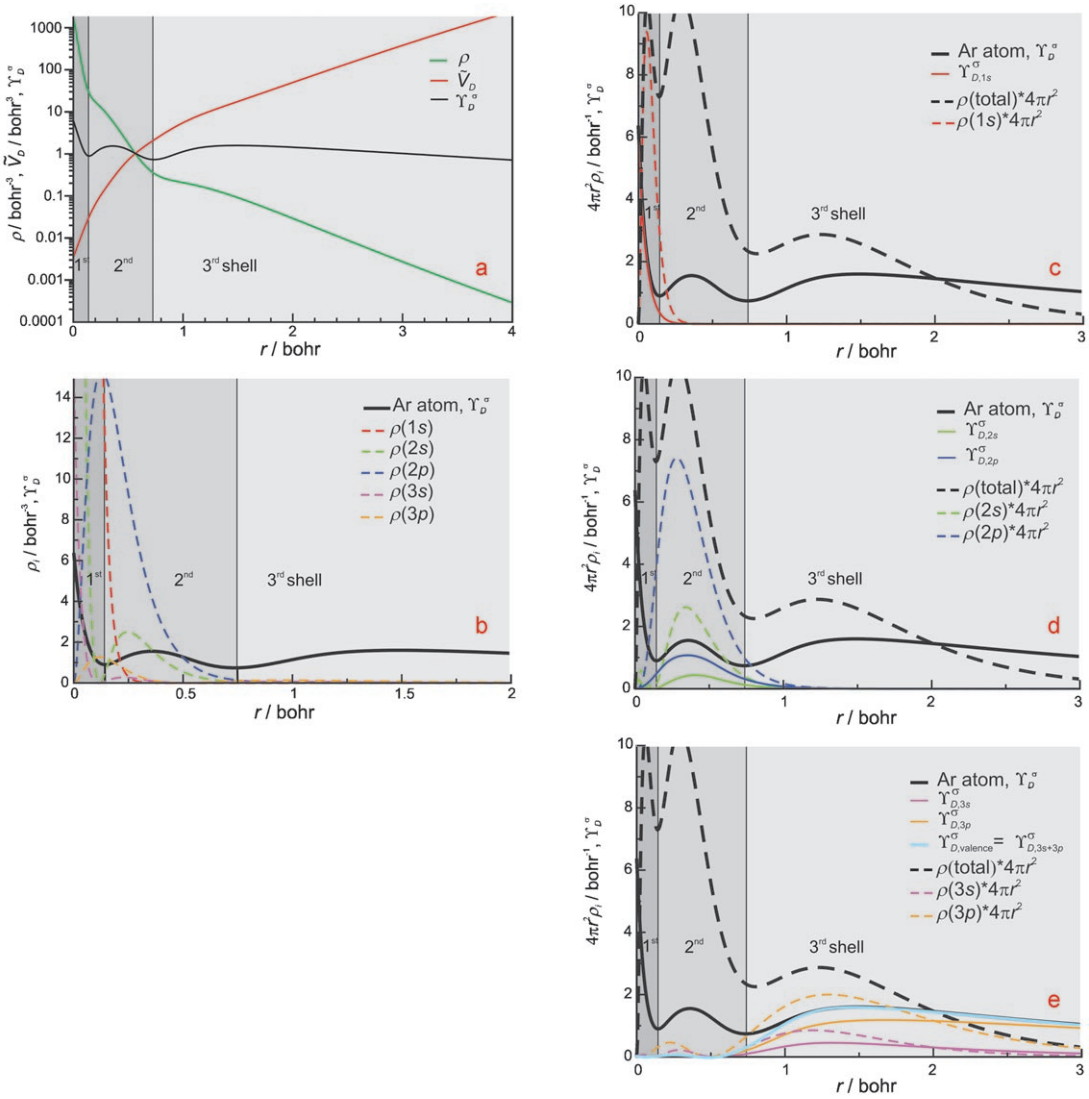


Figure 1. Argon atom: a) radial dependence of the ELI-D, electron density and scaled pair-volume function; b) radial dependency of the ELI-D and orbital densities; c–e) genuine pELI-D contributions and radial orbital density $P(r)$ for the first (c), second (d), and third (e) atomic shell.

dient approximated level of density functional theory using Becke's exchange energy functional[13] and Lee, Yang and Parr's correlation energy functional.[14] All-electron basis sets, in which all electrons were kept unfrozen, of at least triple-zeta quality with two sets of polarization functions (named TZ2P) from the internal library of ADF were used throughout. The results were checked for basis set convergence.

From the HF, Kohn–Sham and CAS wavefunctions obtained the ELI-D and pELI-D contributions were calculated on equidistant grids using the DGrid program,[15] which took maximally 1 hour for each diagram presented.

## Results

In the following, use of the bare functional $\Upsilon_D^\sigma(\boldsymbol{r})$ without ELF-like Lorentzian scaling is advocated as it represents the additive quantity. In fact there is even no need for scaling in graphic applications as the values of the ELI-D in the core regions are typically in the range $0 \leq \Upsilon_D^\sigma \leq 10$, whereas the valence region typically displays values within the range $0 \leq \Upsilon_D^\sigma \leq 2$ (with the exception of hydrogen atoms, since for protons the core and valence region is identical).

**Argon atom**: As the simplest example we chose the representation of the atomic shell structure in position space of the argon atom given by the total ELI-D in a simple $\Upsilon_D^\sigma(\boldsymbol{r})$ versus $|\boldsymbol{r}|$ plot (Figure 1a). Note, the shell-like topology is not depicted by each of its separate ingredients, that is, the electron density and the pair-volume function. For an atom, the size of the pair volumes monotonically increases with radius $r=|\boldsymbol{r}|$ as the curvature of the Fermi hole decreases with $r$.[16] This is due to the limiting behavior of the charge density: at large $r$ a single orbital completely dominates (ionization potential) resulting in vanishing same-spin probability density. Thus, the ELI-D obtains its specific shell-structure shape for an atomic system from the local product of two monotonic but counter-current functions, $\rho$ and $\tilde{V}_D$.

  

The first atomic shell consists of a sphere centered at the nuclear position at which the radius $r_{1s}$ is determined by the position of the first minimum of the ELI-D along $r$. The second shell represents an onion-like-shaped region between two consecutive minima of the ELI-D. The outermost shell extends to an infinite radius. The orbital density contributions are displayed in Figure 1b in a $\rho_i(\boldsymbol{r})$ versus $|\boldsymbol{r}|$ plot. It can be clearly seen that the genuine canonical orbitals for a certain shell (the genuine orbitals for the $n$th shell are those with the same main quantum number $n$) in direct space are not confined to that region, which introduces losses in the electron count for that shell. These losses are compensated by contributions from genuine orbitals of other shells. From an orbital point of view, quantitative shell structure in direct space is due to nearly exact compensation of genuine losses and non-genuine gains of charge contributions within each spatial shell.[17] The orbital and total charge contributions in spherical shells can be displayed along a radial line using the radial charge distribution $P(r)=4\pi r^2\bar{\rho}(r)$, with $\bar{\rho}(r)$ being the spherically averaged charge density in which the two angular components (polar coordinates representation) have been integrated out. The integral of $P(r)$ between two radial positions $r_1$ and $r_2$ directly yields the number of electrons in the enclosed spherical shell region. A comparison of the total and orbital-resolved radial charge distributions with the corresponding total ELI-D and pELI-D can be found in Figure 1c–e. At each point the two orbital-resolved quantities add up to the corresponding total quantity. Use of the summed pELI-D contributions of all the valence orbitals represents a natural and controllable way to define an approximate valence-only ELI-D (cf. Figure 1e). Furthermore, it can be seen that the radial total and orbital-resolved charge distributions for argon have similar topologies to the total ELI-D and pELI-D contributions. Although for the lighter elements up to argon the atomic shell structure is qualitatively represented by $P(r)$, this function starts to fail beyond argon. In contrast, the ELF, and therefore the ELI in the single-determinantal approximation as well, displays the atomic shell structure even quantitatively at least up to xenon.[17,18] From Figure 1c–e it may be tempting at first glance to assume for $\Upsilon_D^\sigma(\boldsymbol{r})$ and $P(r)$ a similar kind of construction principle to define a weighting scheme for the charge density, but this is not the case. Whereas $\Upsilon_D^\sigma(\boldsymbol{r})$ represents a three-dimensional distribution of charges in compact regions, $P(r)$ represents a one-dimensional distribution of charges within spherical regions. For this reason, the construction principle of the radial charge distribution is not transferable to non-spherical systems. In this context the restricted populations approach offers a concept of space partitioning to create physically motivated weighting schemes, for example, for charge density in the case of the ELI-D.

**pELI-D contributions of canonical orbitals—$N_2$ and $F_2$:** Before discussing the ELI-D and pELI-D contributions, a comparison of the same-spin pair volume functions for the isolated atoms and the dimeric molecules is useful. As discussed in the previous paragraph, the pair volume function for an isolated atom displays a monotonic increase with $r$ and the question arises, what happens for a dimeric molecule? As can be seen in Figure 2a the pair volume function displays a $(3,+1)$ saddle point at the midpoint of the internuclear line, that is, it is maximal along the internuclear line (one negative curvature), but minimal (two positive curvatures) perpendicular to it.

The ELI representation of the $N_2$ molecule displays one core attractor for each nitrogen atom, a common valence region with an attractor between the nitrogen atom cores and two other attractors located at the opposite sides of the N–N contact (Figure 2b).

The core regions of both nitrogen atoms are mainly composed of in-phase ($1\sigma_g$) and out-of-phase ($1\sigma_u$) combinations of the 1s orbitals, giving only small pELI-D contributions in the valence region (Figure 3). For topological reasons the attractors in the valence region have been interpreted as bonding and lone-pair attractors, respectively. This is fully consistent with the pELI-D analysis (Figure 3): the ELI-D value for the bonding attractor is created from two bonding orbitals, the $2\sigma_g$ and $3\sigma_g$ orbitals, whose pELI-D contributions indicate an attractor between the nitrogen atoms. In contrast, the orbital electron density between the nitrogen atoms is maximal along the line (in total a $(3,-3)$ attractor) only for the $2\sigma_g$ orbital, but not for the $3\sigma_g$ orbital, for which it is minimal along the line with a $(3,-1)$ saddle point in total.

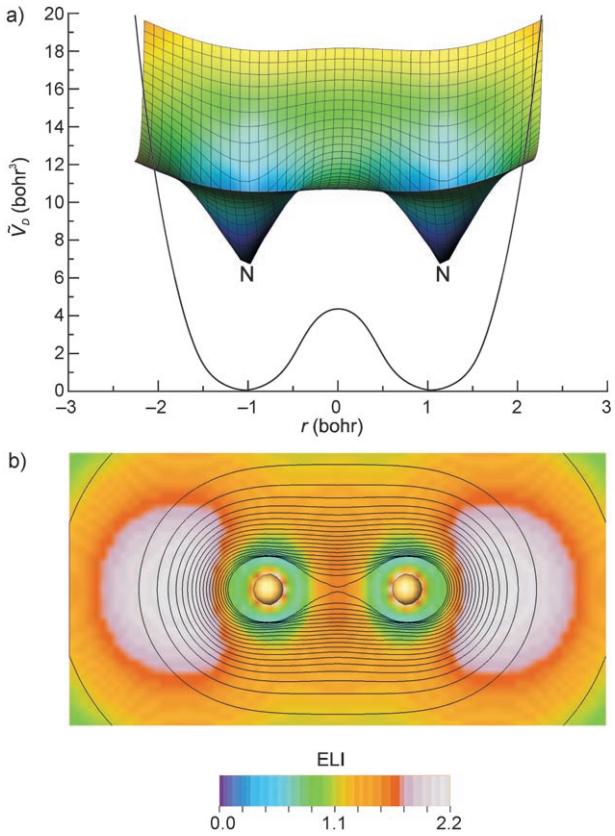


Figure 2. Molecule $N_2$: a) pair volume function; b) total ELI-D, represented by color coding; black contour lines depict the total electron density.

  

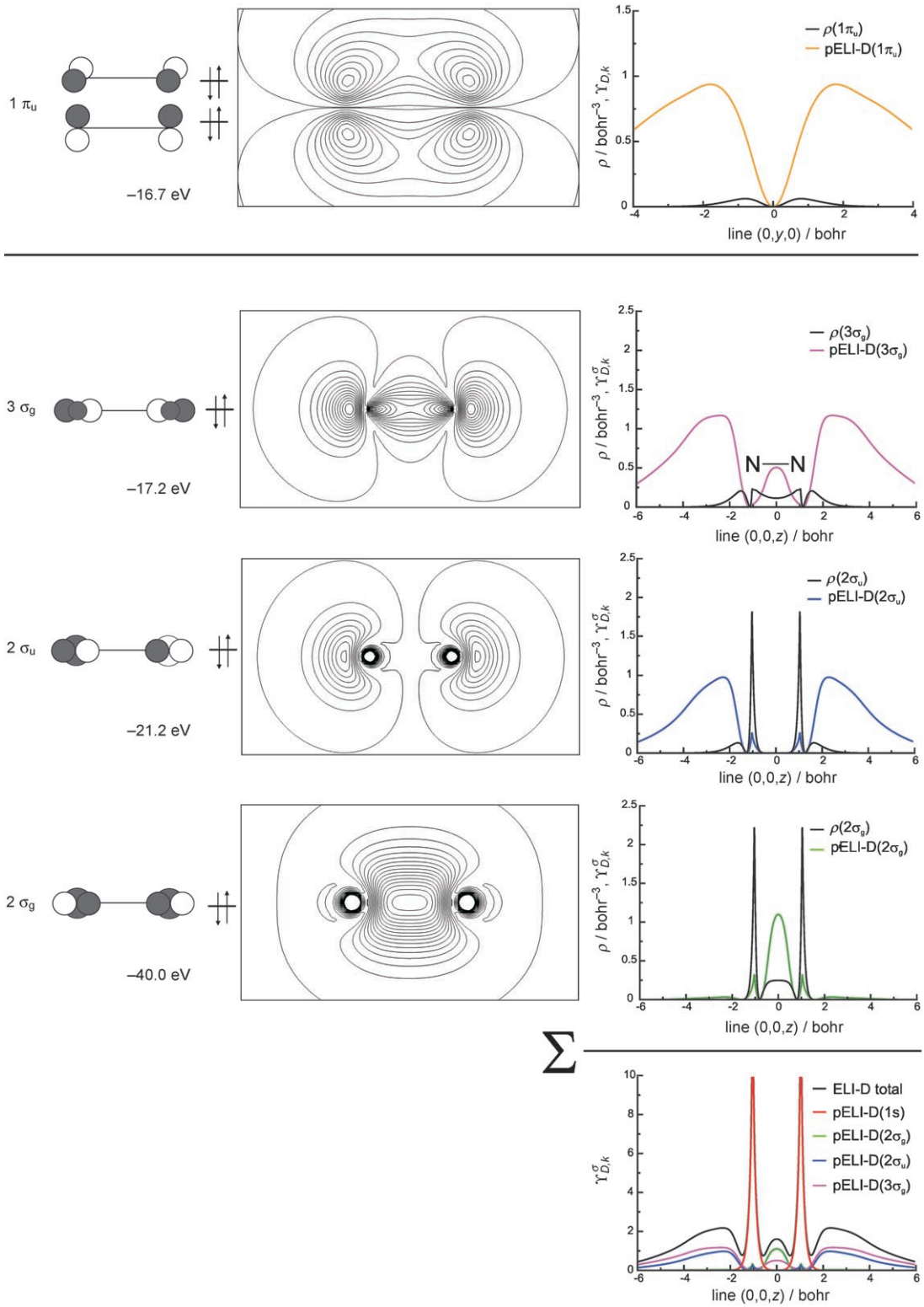


Figure 3. $N_2$ molecule with atoms at $(0,0,\pm z')$, π orbitals (above), and σ orbitals (below). From left to right: canonical orbital schemes, 2D orbital densities and 1D plots of the pELI-D contributions and corresponding orbital densities along the internuclear line (σ orbitals) or perpendicular to it (π orbitals).

The ELI-D attractor value of the lone pair is also composed of two canonical orbital contributions, the $2\sigma_u$ and $3\sigma_g$ orbitals, which both display an attractor of pELI-D close to the total ELI-D lone-pair attractor. Thus, canonical orbital $3\sigma_g$ provides sizable pELI-D contributions for both types of valence attractors, and its topology displays both attractors.

  

Of course, in this simple case similar conclusions can be drawn from an analysis of the canonical orbitals using well-established arguments of second-order mixing between nominal 2*s* ($2\sigma_g$) and $2p_z$ ($3\sigma_g$) bonding orbitals. However, having looked at all the occupied orbitals there is still no picture about what the total wavefunction will look like because the orbitals do not add up to give the wavefunction: it is the orbital densities that add up to give the total electron density. The point to be made here is that the final result of a one-by-one orbital analysis does not give any idea about the total wavefunction and its chemical bonding properties. In contrast, the pELI-D contributions simply add up to give the total ELI-D with no negative contributions. The chemical bonding scenario present in an ELI-D distribution can be easily understood in terms of the constituting orbital pELI-D contributions, which themselves can be reconstructed from the orbital densities and the shape of the weighting pair volume function.

It is now interesting to analyze why no separate attractor for the π-type interaction is found in the ELI-D (and in the ELF) representation of $N_2$. Analysis of the pELI-D along a line running perpendicular to the internuclear line and cutting the bond midpoint (Figure 3, top) clearly shows that the $1\pi_u$ orbitals indeed produce a pELI-D attractor displaced from the bond midpoint, that is, a ring attractor, in this case of cylindrical symmetry, of the molecule. However, the sum of the pELI-D contributions from the $2\sigma_g$ and $3\sigma_g$ orbitals is greater at the bond midpoint than at the π-type attractor position and, therefore, this pELI-D attractor is concealed in the total ELI-D (Figure 4a–c). As pELI-D contributions are always positive this is a representative example of the general mechanism, how pELI-D topologies can be concealed in the total ELI-D. As an indication of such a scenario, it should be noted that at the bond midpoint the absolute value of the curvature of the total ELI-D in a perpendicular direction is much reduced compared with the constituent pELI-Ds (see Figure 4d). Thus, from a purely topological point of view this situation is not too far from topological instability. Although results from highly correlated calculations indicate that $N_2$ will keep its ELI-D topology, it would not be surprising if an isoelectronic molecule displayed a ring attractor instead, and, indeed, this scenario occurs with acetylene.

On proceeding to $F_2$, it is instructive to analyze how the subsequent filling of antibonding orbitals changes the topology of the ELI-D. For $F_2$ the π-antibonding orbitals ($1\pi_g$) are completely filled such that in the simple MO picture the single bond survives. The ELI-D (and the ELF) computed from the HF wavefunction displays a single attractor at the bond midpoint, whereas the ELI-D (and the ELF) from the DFT calculation displays a shallow two-attractor structure between the atoms (Figure 5a). Although at first glance these results look like quite different, a closer look at the curvature of the ELI-D (HF) at the bond midpoint reveals that the attractor is extremely flat having nearly zero curvature along the internuclear line (Figure 5b). This scenario is caused by the significant two-attractor structure of $2\sigma_u$

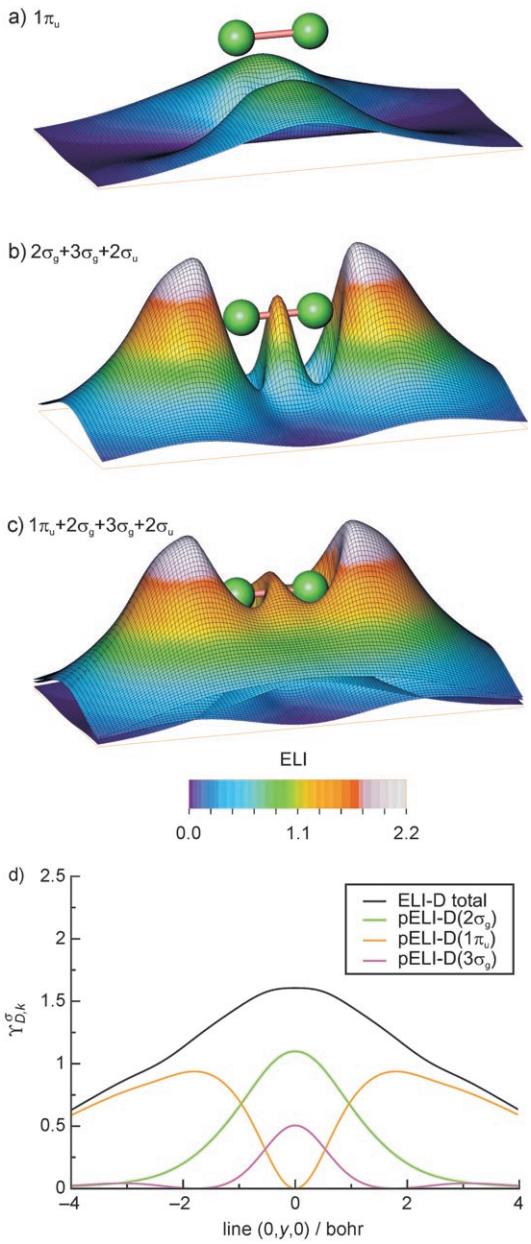


Figure 4. Molecule $N_2$: 2D pELI-D orbital contributions in combined height field/color code representation for a) $1\pi_u$, b) the sum of $2\sigma_g+2\sigma_u+3\sigma_g$ contributions, c) the sum of $1\pi_u+2\sigma_g+2\sigma_u+3\sigma_g$ contributions, and d) 1D pELI-D orbital contributions along a line cutting the bond midpoint and running perpendicular to the internuclear line.

pELI-D contributions, which are just concealed by the slightly prevailing single-attractor pELI-D contributions of $3\sigma_g$, whereas $2\sigma_g$ is already quite flat (Figure 5b). The pELI-D contributions of the DFT orbitals (not shown) are qualitatively similar, but the $3\sigma_g$ pELI-D contributions are not dominant enough along the internuclear line to completely conceal the $2\sigma_u$ two-attractor structure and it survives in the total ELI-D (and in the ELF). The decision about which of the two ELI-D topologies is the correct one can be made on the basis of a definitively better wavefunction. It is already known that a completely active space (CAS) calculation for

  

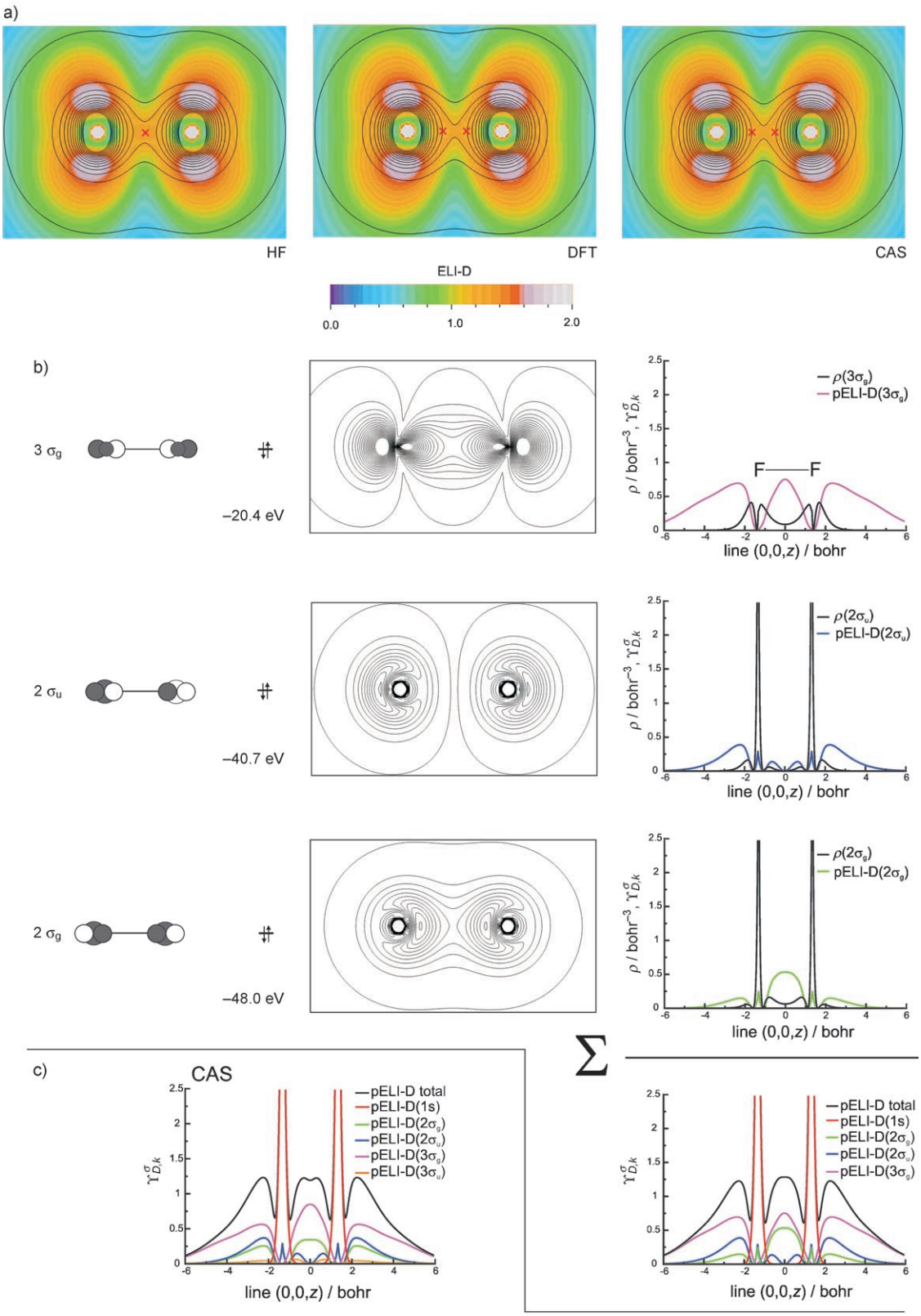


Figure 5. $F_2$ molecule with atoms at $(0,0,\pm z')$: a) the total ELI-D (from different wavefunctions) depicted by color coding in the molecular plane. The two-attractor structure is barely visible and therefore marked by red crosses; black contour lines depict total electron density. b) Left to right: canonical orbital diagrams, orbital densities and 1D pELI-D and density contributions of σ orbitals along the internuclear line (HF wavefunction). c) Natural orbital pELI-D contributions from CAS calculation.

  

$F_2$ using all 14 valence electrons within eight active orbitals (i.e., the $\sigma^*p_z$-antibonding $3\sigma_u$ natural orbital is allowed to become fractionally occupied at the expense of the initially completely filled ones) displays the two-attractor feature in the ELI.[6] As this result is also consistent with results obtained at higher correlated levels (MRCI-SD) we restrict our discussion here to the ELI-D calculated from the initial CAS(14,8) wavefunction.[6] In this case the pELI-D orbital density contributions are computed from the natural orbitals (Figure 5b) which are allowed to have fractional occupation numbers. Indeed, $3\sigma_u$ is populated by 6% and mainly the $3\sigma_g$ orbital is getting depopulated. As a result the pELI-D contributions from $3\sigma_g$ are no longer dominant enough to conceal the two-attractor pELI-D structure from $2\sigma_u$ along the internuclear line. Additionally, the $3\sigma_u$ pELI-D contributions also display a two-attractor structure. As a result a bifurcated attractor[6] between the fluorine atoms is obtained, which is consistent with a weakened bond scenario in accord with its relatively low dissociation energy.

$N_2$ and $F_2$ have different topologies along the internuclear line even though the same orbitals contribute to this line because the additional $1\pi_g$ orbitals have a nodal line there. The different ELI topologies along the internuclear line can be traced back to the different orbital densities because the respective pair volume functions are quite similar. However, use of just the orbital densities for bonding analysis would not be feasible as there has to be a measure that allows extraction of the significant differences. This is achieved through the weighting pair volume function that defines the pELI-D contributions and the ELI-D in total. As discussed above, the observed two-attractor feature of the ELI for $F_2$ is clearly caused by the orbital density of the σ antibonding orbital $2\sigma_u$ (Figure 5b). The reason for this is the mainly 2s–2s antibonding nature of this orbital which has fewer admixtures of $2p_z$ contributions than $N_2$. Compared with $N_2$ this leads to significantly smaller pELI-D contributions to the lone-pair region and to a pELI-D topology between the atoms dominated by the 2s–2s orbital combination. For $N_2$ the orbital mixing between the nominal s and p orbitals is stronger owing to a smaller energy difference and thus the sizable admixture of $2p_z$ character in the $2\sigma_u$ orbital largely cancels the 2s–2s character between the atoms and the two-attractor feature of the $2\sigma_u$ pELI-D does not occur in the total ELI-D (Figure 3).

Turning to the π orbitals it can also be seen that the pELI-D contributions of the bonding $1\pi_u$ orbitals have a different topology for $F_2$ compared with $N_2$. They are represented by two symmetrical ring attractors (Figure 6b) and not just one surrounding the midpoint of the internuclear line as for $N_2$ (Figure 4a). Thus, the combination of the bonding and antibonding π orbital pELI-D contributions results in a deep and rather flat valley between the atoms and rather pronounced ring attractors approximately surrounding each atomic core (Figure 6c). This has consequences for the representation of the lone-pair region, which is different for $N_2$ and $F_2$. Although in $N_2$ the location of the lone-pair attractor was determined by σ contributions, the ELI topology of the lone-pair region for $F_2$ was finally determined by the π orbitals which effectively conceal the smaller contributions of the σ orbitals away from the internuclear line (Figure 6d). As a result, the lone-pair feature is represented by two ring attractors located slightly on the bond-opposed side of the molecule (Figure 6e).

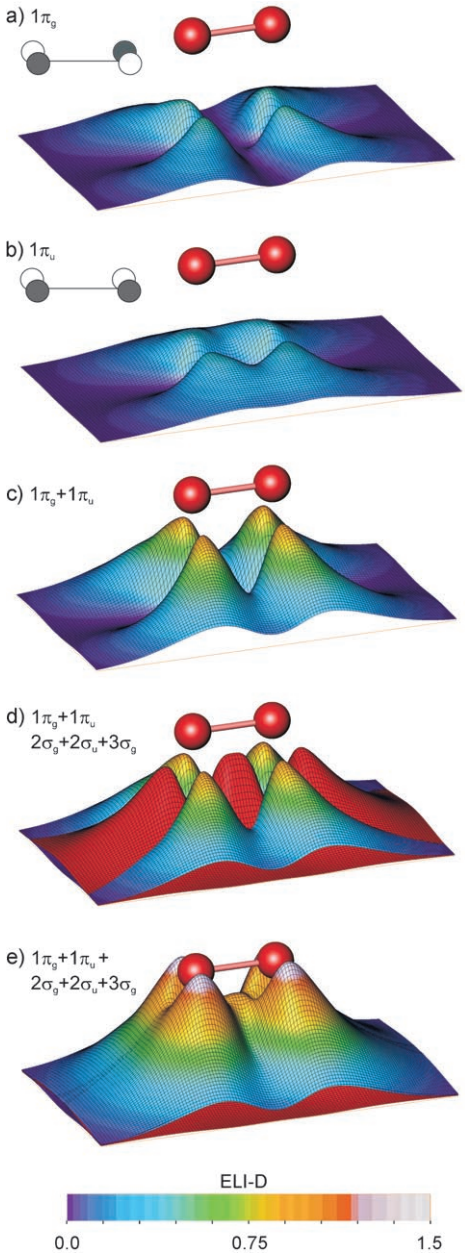


Figure 6. Molecule $F_2$: formation of lone-pair regions due to π orbital dominance. Combined height field/color code visualization of the pELI-D contributions in the molecular plane for a) π*, b) π, c) sum of π+π*, d) comparison between total σ-type (red) and π-type contributions, and e) the ELI-D for all valence orbitals.

**pELI-D contributions of localized orbitals—$C_2H_4$ and $C_6H_6$:** The C–C double bond for ethylene is represented by two equivalent ELI-D (and ELF) attractors above and below

  

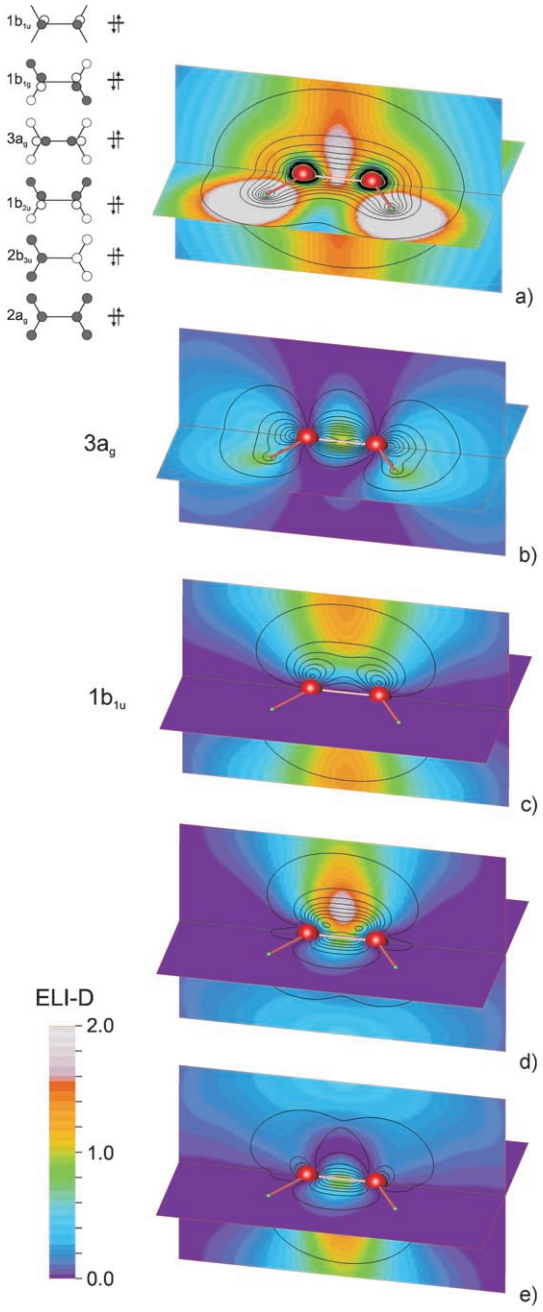


Figure 7. Canonical orbital versus localized orbital pELI-D contributions for the $C_2H_4$ molecule: a) total ELI-D; b) pELI-D for $\sigma p_z$ orbital $3a_g$; c) pELI-D for $\pi$ orbital $1b_{1u}$; d) pELI-D for one localized "banana bond" orbital front side; e) pELI-D for the second localized "banana bond" orbital back side. Partial pELI-D contributions are represented by a color map, black contour lines depict the corresponding electron density.

the molecular plane (Figure 7a) and not by separate σ- and π-type attractors, as may be expected from canonical molecular orbitals. The pELI-D and orbital density contributions of the canonical σp and πp bonding orbitals $3a_g$ and $1b_{1u}$ are represented in Figure 7b,c. It can be seen that the pELI-D topology displays the expected bonding features consistent with the orbital diagram, but not until all contributions of the canonical orbitals have been added can the final topology in certain regions of space be obtained. For this purpose, localized orbitals can be utilized instead of the canonical ones. However, within the framework of localized orbitals, some orbital localization schemes (e.g., Foster–Boys localization[19]) display the so-called "banana bond" representation, that is, two similar localized orbitals for the C–C bond, whereas others display σ–π separation (Edmiston–Ruedenberg localization[20]). The classical orbital localization procedures correspond to a unitary transformation of the occupied orbitals that fulfil some imposed localization condition. Although all these localization schemes are conceptually different, they can be considered physically equivalent and non-unique since the total energy is invariant against such orbital rotations. The ELI is invariant against such orbital rotations as well. From the viewpoint of the total ELI-D topology, it can be useful to analyze the orbital representation whose pELI-D contributions depict the final ELI-D topology in certain regions of space.

For ethylene, Foster–Boys-localized MOs display two equivalent "banana bonds" whose pELI-D contributions are shown in Figure 7d,e. It can be seen that the banana bond feature of the pELI-D of these localized orbitals is indeed recovered in the total ELI-D. In contrast, the localized orbital density topology, which shows a two-attractor structure in the plane perpendicular to the nuclear plane (black contour lines in Figure 7d), is not recovered in the total density (black contour lines in Figure 7a).

For benzene, the electronic structure in terms of canonical orbital diagrams, orbital densities and pELI-D contributions is displayed in Figure 8 for all 15 occupied valence orbitals. Detection of the bonding character from the orbital density alone is not an easy task, whereas the pELI-D is easy to understand. Different situations can be recognized for the separate orbital contributions: multi-center bonding ($2a_{1g}$, $3a_{1g}$), two-center σ bonding at the internuclear line ($2e_{1u}$, $3e_{2g}$) and displaced from it ($2e_{2g}$, $1b_{2u}$, $3e_{1u}$), and π bonding with attractors above and below the atomic plane ($1a_{2u}$, $1e_{1g}$). The topology of the final ELI distribution (Figure 9a) is difficult to predict just from inspection of the diagrams. Therefore, analysis in terms of localized orbital distributions is much more transparent. However, besides the non-uniqueness of the localization condition another difficulty arises for certain electronic situations, namely near or exact localization degeneracy of localized orbital sets.[21] Foster–Boys-localized orbitals for benzene display an alternating pattern of single bonds and "banana bonds" which provides an illustrative example of a discrete doubly degenerate set. As already demonstrated for ethylene, Foster–Boys localization exhibits a preference for "banana bonds" and the localized orbitals of the double bonds of benzene could be expected to be displayed in the same way. But as the double bonds are conjugated, only three canonical π orbitals are occupied. The bonding pattern obtained for the nine C–C bonding localized orbitals consists of alternating three localized single bond orbitals with pELI-D attractors at the C–C bond midpoint and six "banana bonds" with attractors above and below the remaining three C–C contacts.

  

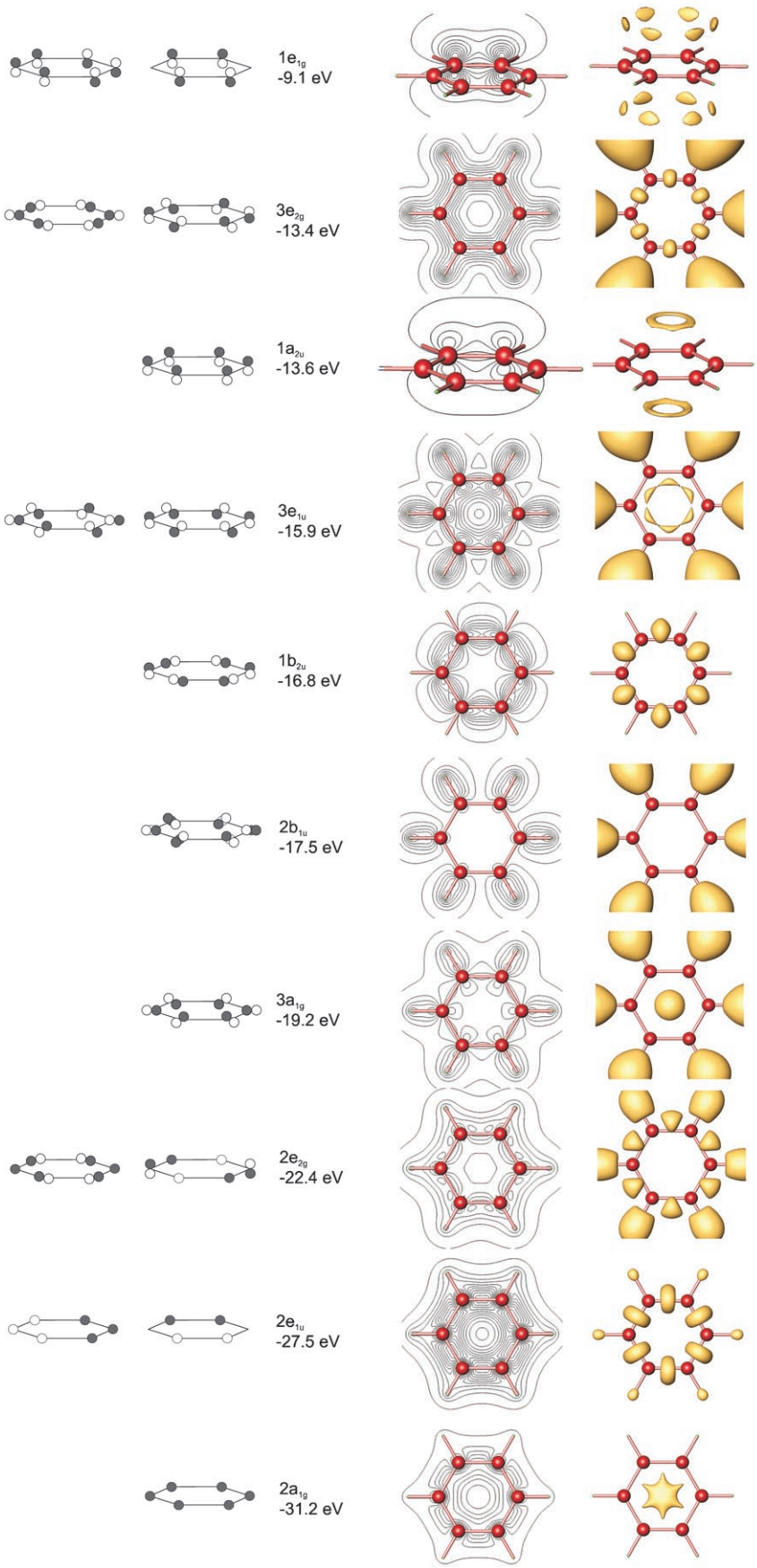


Figure 8. Molecule $C_6H_6$: left to right: orbital diagrams, orbital densities and pELI-D orbital contributions for each irreducible representation of all the valence orbitals.

The pELI-D contributions of the three separate localized orbitals, one single bond and two banana-type bonds, are depicted in Figure 9b. Although this pattern resembles the Kekulé structure having $D_{3h}$ symmetry, it has a different meaning here as the total electron density and the total ELI-D still have the correct $D_{6h}$ symmetry. The reason for this is that the tails of the "banana bond" orbitals account for the "missing" electron density of the localized single bond orbitals in order to yield a fully symmetrical electron density. Indeed, inspection of the spread of the localized orbitals $\Delta = <\boldsymbol{r}^2> - <\boldsymbol{r}>^2$ reveals that the banana bond orbitals have a roughly 40% larger spread than the localized single bond orbitals. The color coding of the pELI-D isosurfaces in Figure 9b is a measure of the dominance of the pELI-D (or orbital density) contributions at each point of the isosurface with respect to the total ELI-D (or density). It indicates that the pELI-D (density) fraction in the region of the single bond localized orbital decreases quite rapidly with increasing distance from the molecular plane to values of only about 0.5. In contrast, for each "banana bond" orbital this contribution at first increases with increasing distance from the molecular plane. In Figure 9c,d the corresponding situation is quantified along a line in the $z$ direction through the bond midpoint. The single bond pELI-D contribution is well localized around the ELI-D attractor, but its dominance rapidly decreases from the bond midpoint and the tails of the four less localized banana bond orbitals strongly dominate beyond $|z| \gg 1.6$ bohr (85 pm).

In the total ELI-D representation the bonding between the carbon atoms is characterized

  

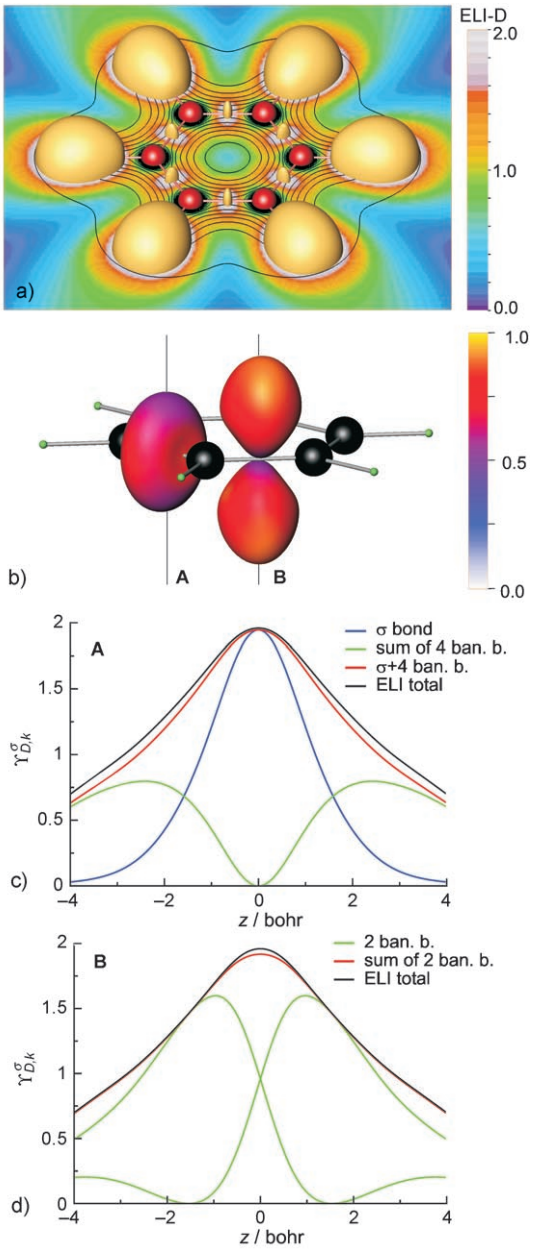


Figure 9. Molecule $C_6H_6$: a) the total ELI-D using 1.86-localization domains to display the C–C attractor location along the internuclear line; b) separate pELI-D contributions for three localized orbitals: one single bond and two banana bond contributions; the color coding depicts the fraction of the respective orbital pELI-D (density) contribution relative to the total ELI-D (total density) as a function of position; c) pELI-D through the σ bond (line A in Figure 9b); d) pELI-D through the midpoints of two banana bonds perpendicular to the molecular plane (line B in Figure 9b) reveals the "banana bond" feature is concealed upon summation of the two "banana bond" contributions, as displayed by the total ELI-D.

by a single attractor at the internuclear line between the nearest carbon atoms. This obvious difference to ethylene can be traced back with the help of localized orbitals. Although decomposition of the total ELI-D into the above described localized orbital contributions (Figure 9b) suffers from the already mentioned artifacts, it is clear that the banana bonds must be different in ethylene and benzene: in contrast to ethylene, addition of just the two banana bond pELI-D contributions, as shown in Figure 9d, conceals the banana bond topology and creates an attractor in the nuclear plane. This is due to the strong overlap of both the pELI-D contributions, which can also be seen from the color-coded pELI-D isosurface in Figure 9b. Note, the different representation of the C–C bond in the total ELI-D is not only a result of the longer C–C distance because an independent calculation on ethylene using the C–C distance of benzene reveals that the "banana bond" feature survives in the total ELI-D. Therefore, it is interpreted as being a result of the weaker π bond character in benzene.

So far, both the strength and the weakness of currently used localized orbital schemes applied in bonding analysis within the framework of orbital-resolved ELI-D analysis has been exemplarily shown. Clearly there would be an interest in a type of localized orbital or function that shows the same topology as the total ELI-D itself, not only because of the problems of non-uniqueness and localization degeneracy, but also because the ELI-D represents a physical measure of electron localization.[3] In contrast to those localized orbitals currently used, this new type would in general not be restricted to integer occupation numbers even for a single-determinantal wavefunction as the number of ELI attractors is not related in a simple way to the number of building MOs, as exemplified above for benzene.

**Penultimate shell structuring—$Sc_2^{2+}$ and $TiF_4$**: For a given single-determinantal wavefunction, the ELI-D gives the same topology as the ELF. However the ELF distributions have to be re-interpreted in terms of the ELI-D in order to enable charge decomposition analysis. In this section the charge decomposition analysis of the ELI-D applied to $Sc_2^{2+}$ and $TiF_4$ molecules serves to discuss previously published studies[22,23] on penultimate-shell structuring of the ELF for transition-metal atoms. Both studies have been performed using DFT methods and we will therefore explicitly discuss and display our DFT results.

Within the framework of the ELF, the occurrence of penultimate-shell structuring in transition-metal species due to participation of that shell's genuine orbitals (i.e., atomic orbitals with the same main quantum number as the shell number) in covalent bonding interactions has been discussed in detail in relation to metal–metal interactions.[22] It was shown for the $Sc_2^{2+}$ molecule in the $^1\sum_g^+$ electronic state that an attractor in the fourth atomic shell region occurs even though only genuine orbitals of the penultimate shell (i.e., 3s, 3p and 3d orbitals of the third atomic shell) are populated. This is due to the ambivalent character of the 3d orbitals of transition metals: on the one hand they are genuine orbitals of the third shell, but on the other hand they may make significant contributions to the fourth shell as a result of chemical bonding. With the aid of orbital-resolved pELI-D contributions it is now possible to gain a deeper insight into the problem.

  

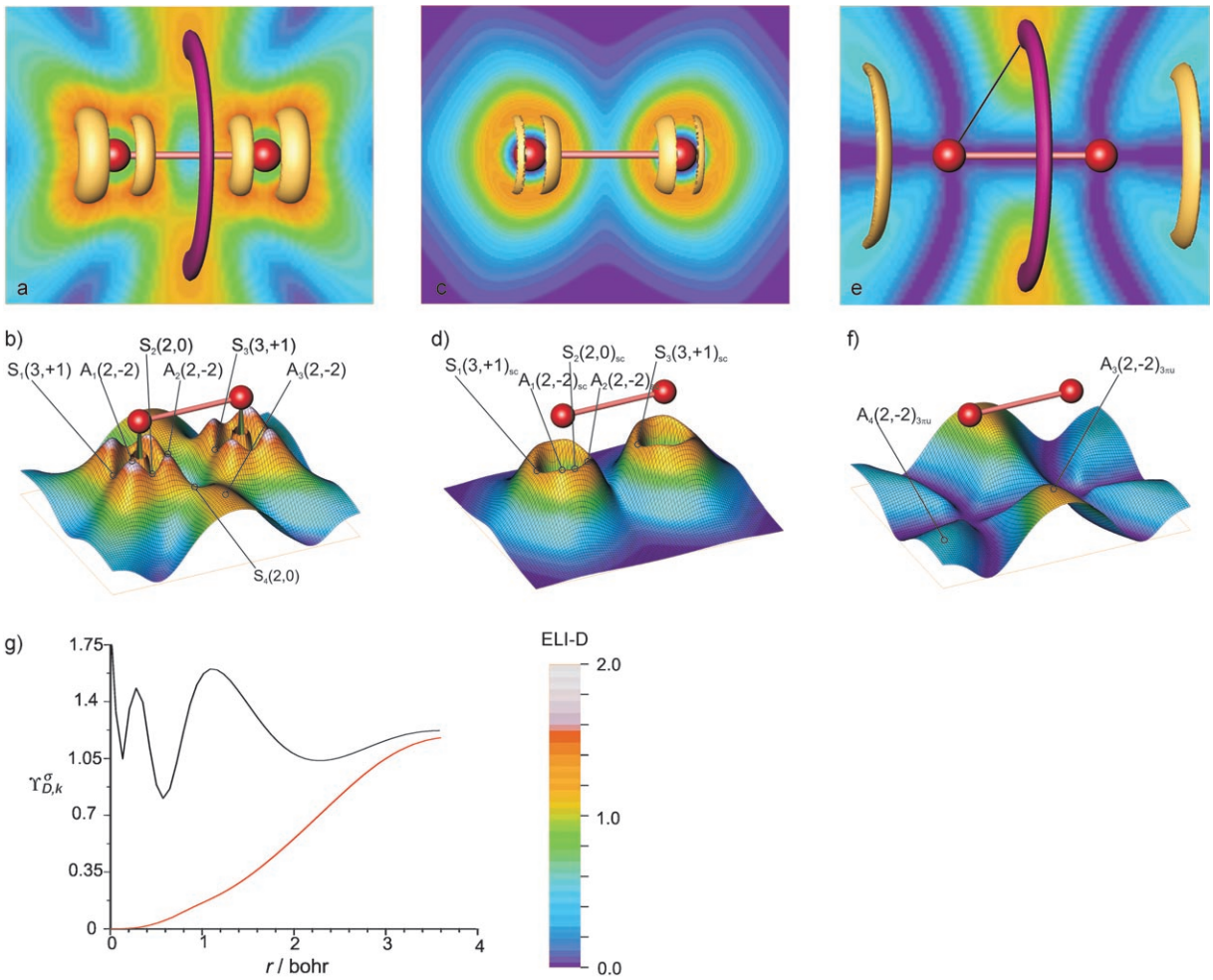


Figure 10. Molecule $Sc_2^{2+}$: ELI-D and pELI-D contributions in the atomic plane depicted by color coding and either localization domains (a,c,e) or height field representation (b,d,f): a) the total ELI-D third-shell structuring is indicated by brown 1.51-localization domains, the ring-shaped π-bonding attractor in the fourth shell is signified by purple 1.21-localization domains; b) the total ELI-D topology: attractor $A_i$ and saddle point $S_i$ locations; c) pELI-D contributions for semicore orbitals employing 1.39-localization domains; d) semicore orbitals' pELI-D topology: attractor and saddle point locations; e) pELI-D contributions from HOMO $3\pi_u$ providing πdd bonding; two types of ring attractors are signaled by brown (0.57) and purple (1.18) localization domains; f) $3\pi_u$ pELI-D topology: attractor locations; g) pELI-D contribution from the $3\pi_u$ orbital (red line) and the total ELI-D (black line) along a straight line from the nucleus to the ring attractor in the fourth shell (see black line in Figure 10e).

The orbital sequence beyond the atomic L shell for this molecule is $4\sigma_g(\sigma 3s, -63.1\ eV)$, $4\sigma_u(\sigma^*3s, -62.5\ eV)$, $5\sigma_g(\sigma 3p_z, -43.2\ eV)$, $2\pi_u(\pi 3p_{x,y}, -42.5\ eV)$, $2\pi_g(\pi^*3p_{x,y}, -42.1\ eV)$, $5\sigma_u(\sigma^*3p_z, -40.8\ eV)$, $3\pi_u(\pi 3d_{xz,yz}, -14.2\ eV)$ and the eight nominal 3s and 3p MOs will be referred to below as semicore states (sc).

The features displayed by the ELI-D (and the ELF) are a significant structuring of the penultimate (third) shell via two ring attractors and one additional ring attractor in the valence region (Figure 10a). Until now, no numerical measure has been given to the structuring. We propose a structuring index based on the ELI-D values of the penultimate-shell critical points as follows. Figure 10b shows a three-dimensional plot of the ELI-D (the height is proportional to the value of the ELI-D) in one molecular plane, which, as a result of cylindrical symmetry, contains all the necessary and sufficient information about the ELI-D topology of this molecule. The penultimate shell of each scandium atom displays two different ring attractors $A_1$ and $A_2$ and three different saddle points $S_1$, $S_2$ and $S_3$. One further ring attractor $A_3$ is located in the valence shell and a ring-shaped saddle point $S_4$ connects $A_2$ and $A_3$. A structuring index for the penultimate shell is defined for the purpose of quantitative discrimination between a spherical free atom with spherical and closed ELI-D isosurfaces at any intrashell value and those atomic species that display open isosurfaces (e.g., with holes, rings) for certain intrashell isosurface values. The decreasing sequence of intrashell critical-point ELI-D values $A_1 > A_2 > S_2 > S_3 > S_1$ defines the isosurface shape evolution as the isosurface values decrease. This can be easily understood from Figure 10b by considering a cutting plane parallel to the molecular plane that is moved downward from large heights (large ELI-D isosurface values) and by bearing in mind the cylindrical symmetry: the first structure of the third (penultimate) shell appears at height $A_1$ where a ring attractor for each scandium atom appears. On further lower-

  

ing the value a second ring attractor for each scandium atom appears at value $A_2$. For each scandium atom the two separate rings fuse at value $S_2$ into one ring, which still has two holes along the internuclear line. At value $S_3$ the neighbor-directed hole closes and at $S_1$ the backside hole closes. From this value on, the isosurface for each scandium atom's penultimate shell is fully closed. In Figure 10b this would correspond to a situation where an imagined horizontal cutting plane reveals within the penultimate shell region a closed line surrounding each scandium atom. We propose to use the difference in the ELI-D values between the first occurrence of a structure $A_1$ (i.e., the highest attractor) and the vanishing of the last structuring feature $S_1$ (i.e., the lowest saddle point) as the definition of the structuring index $\varepsilon = A_1 - S_1 = 0.49$.

The semicore pELI-D contributions (Figure 10c,d) show qualitatively the same kind of structuring as the total ELI-D, however, in a significantly reduced amount: the pELI-D value $A_{1,sc} = 1.41$ is found for the dominant ring attractor and for the lowest saddle point $S_{1,sc} = 1.21$, which gives $\varepsilon = 0.20$. The structuring of the semicore states' pELI-D contributions is already a signature of significant orbital interaction between them, which is also corroborated by the noticeable orbital energy differences (see above) between the bonding and antibonding semicore MOs. Noteworthy, none of the separate ingredients of the ELI, neither the semicore orbital density nor the pair volume function alone, displays the type of structuring observed.

The remaining 60% of the total structuring of the penultimate shell is produced by the 3d–3d interaction mediated by the $3\pi_u$ orbitals (Figure 10e,f). It can be seen that the $3\pi_u$ orbitals' pELI-D contributions to the structuring are negligible at the saddle points $S_{1,sc}$, $S_{2,sc}$, $S_{3,sc}$ owing to the orbitals' nodal structure, whereas attractors $A_{1,sc}$, $A_{2,sc}$ are strongly enhanced. At position $A_{1,sc}$ a value of $\Upsilon_D^{\sigma}(3\pi_u) = 0.29$ is found, which leads to the observed final structuring.

By plotting the $3\pi_u$ orbitals' pELI-D contributions along a line from the nucleus to the ring attractor between the atoms in the fourth shell (Figure 10 g), it can be seen that they increase monotonically instead of also possessing an attractor in the third shell, as was initially assumed.[22] The reason for this assumption was the hypothesis that the filled 3s3p semicore states for $Sc_2^{2+}$ would not display an ELF structuring by themselves, which is not true as we now find. Thus, for a strongly covalent interaction the situation can be even more extreme than thought before, namely that the pELI-D contributions of the 3d orbitals may reach out into the valence shell even without displaying an attractor in their genuine shell.

A different situation is met for $TiF_4$. In their work on the geometries of $3d^0$ transition-metal molecules Gillespie et al.[23] investigated the connection between the spatial arrangement of the penultimate (third shell) ELF basins and the arrangement of the ligands. In their discussion the terms "core", "core electrons", "core basins" and "outer-core shell basins" correspond to features of the third atomic shell. Specifically, for $MF_n$ molecules such as $TiF_4$ and $CrF_6$ it was emphasized that the ligands are situated opposite the penultimate-shell basins (ligand-opposed (LO) geometry) "so that they have a minimum interaction with the core". Furthermore it was argued that "the Pauli repulsion between the ligand and the core electrons localizes a pair of opposite-spin electrons at as great a distance as possible from the ligand, that is, in the LO positions, which corresponds in the ELF picture to the LO core basins." Although it is not the scope of this paper to discuss their approach to explaining the geometry of $d^0$ molecules, in the present context a different interpretation of the location of the "outer-core shell basins" (which we prefer to term "penultimate-shell basins" because the third atomic shell is not a true core shell for titanium) and their chemical meaning arises.

For $d^0$ transition-metal-containing molecules, for example, $TiX_4$ and $CrX_6$ ($X$ = F, Cl, Br, ...), the MOs obtained from a HF or Kohn–Sham DFT calculation are consistent with the picture from qualitative MO theory revealing that only bonding metal(3d)–ligand(s,p) orbitals are occupied. The greater the electronegativity difference between the metal and the ligand the more dominant is the ligand majority state character of these orbitals. Antibonding interactions are found through small admixtures of fully occupied metal 3s and 3p semicore orbitals in ligand majority states. A different situation occurs for formally $d^n$ transition-metal molecules as the transition-metal majority d orbitals are occupied and they are significantly metal–ligand antibonding depending on the degree of itineracy. In fact, it is well known that covalency increases, for example, along the series $CrF_3$, $CrF_4^{2-}$ and $CrF_6$, the $d^0$ molecule being the most covalent.[24] All this seems to be in contrast to the interpretation of the ELF topology given by Gillespie at al.,[23] in which ligands were found to prefer positions opposite the ELF core basins so that "unfavorable interactions with the metal core are minimized" neglecting the role of covalent F–Ti interactions completely. We therefore investigated the origin of the penultimate-shell attractor creation and location with the aid of orbital decomposition of the total ELI-D, as illustrated with $TiF_4$.

$TiF_4$ has 16 occupied valence orbitals (i.e., without metal semicore states) whose energy increases in the order $5a_1$, $4t_2$, $5t_2$, 1e, $6a_1$, $6t_2$, $1t_1$, all of them being classifiable as ligand majority states. The Ti(3s,3p) semicore states are found in orbitals $\{4a_1, 3t_2\}$, which lie about 30 and 10 eV lower than the nominal F(2s) MOs $\{5a_1, 4t_2\}$.

The total ELI-D reveals a structuring of the titanium penultimate shell (Figure 11a) as described by Gillespie at al.[23] As a measure of the structuring we use again the difference $\varepsilon$ in the ELI-D values at critical points as described above. The values obtained for the present calculation are about 1.65 and 1.43, respectively, which gives $\varepsilon = 0.22$. The pELI-D computed from the Ti(3s,3p) orbitals $(4a_1 + 3t_2)$ reveals attractors and low-lying saddle points with values at the positions of ELI-D critical points of about 1.28 and 1.27, respectively, yielding very small contributions to the structuring index of about 0.01. In fact there are only two orbital sets that give significantly structured contributions to $\varepsilon$ for the

  

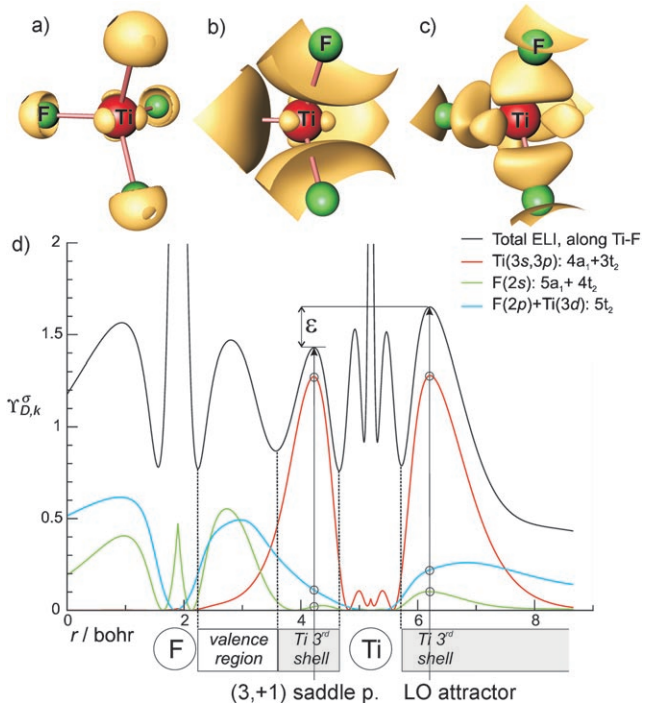


Figure 11. Molecule $TiF_4$: a) the total ELI-D displaying the titanium third-shell structuring using 1.54-localization domains; b) titanium third-shell structuring from the pELI-D contributions of nominal F(2s) orbitals ($5a_1+4t_2$) employing 0.08-localization domains; c) titanium third-shell structuring from the pELI-D contributions of F–Ti bonding orbitals $5t_2$ employing 0.20-localization domains; d) 1D pELI-D contributions along the internuclear line from fluorine (left side) to titanium and beyond; the points at which contributions to the structuring index $\varepsilon$ were measured are indicated by hollow circles. To the right of titanium, the contribution from $5t_2$, which is twice as large as that from $5a_1+4t_2$, is seen to dominate the penultimate-shell structuring.

total ELI-D pattern (Figure 11b,c). One of them is the pELI-D contribution from the $5a_1+4t_2$ orbitals, which are mostly F(2s)-like. The interaction between Ti(3s,3p) and F(2s) can be regarded as a closed-shell interaction in which the energetically lower nominal Ti(3s,3p) MOs $\{4a_1,3t_2\}$ display bonding admixtures of F(2s) and the nominal F(2s) MOs $\{5a_1,4t_2\}$ display antibonding admixtures of Ti(3s,3p). In sum this interaction is therefore antibonding. The pELI-D contributions from the complete set of closed-shell interaction orbitals $4a_1+3t_2+5a_1+4t_2$ can be considered to represent the repulsive part of the orbital interactions. As can be seen from Figure 11d in which different pELI-D contributions are displayed along the internuclear line F–Ti, these interactions (mainly $5a_1+4t_2$) give rise to a structuring contribution to $\varepsilon$ of about 0.09, which is only about 40% of the total structuring $\varepsilon=0.22$ (measured at positions of the total ELI-D attractors and saddle points utilized for $\varepsilon$). The pELI-D contributions from the ligand-directed $5t_2$ orbitals display disynaptic attractors F–Ti and titanium penultimate-shell attractors at the bond-opposed side at values higher than the $5a_1+4t_2$ ones (Figure 11c). They contribute a value of 0.11 to the structuring index. It is these F–Ti bonding $5t_2$ orbitals that make the largest pELI-D contributions to the observed strong structuring of the titanium penultimate shell (Figure 11d). The remaining contributions (0.02) to $\varepsilon$ arise from fluorine lone-pair-type orbitals in which the titanium 3d orbitals do not significantly participate.

Note, the F–Ti disynaptic attractors are concealed in the total ELI-D and from Figure 11d it can be deduced that already the pELI-D contributions from the titanium semicore $4a_1+3t_2$ orbitals conceal the bonding topological feature from $5t_2$ by comparing twice the value at the crossing point of both curves in the valence region with the sum of them at the position of the $5t_2$ pELI-D attractor near by. In this sense it is the observed strong structuring of the penultimate shell on the bond-opposed side that reflects the concealed F–Ti bonding feature. Thus, the appearance and the locations of the titanium penultimate-shell attractors are mainly (50%) a result of a ligand–Ti(3d) covalent interaction and to a lesser extent (40%) a result of a closed-shell interaction between the ligand and the titanium semicore orbitals.

## Conclusion

Application of the restricted populations approach has made it possible to reformulate the original ELI-q functional, defined as the number of same-spin electron pairs per fixed charge, into a new one, the ELI-D, which is proportional to the charge per fixed fraction of a same-spin electron pair. Only the latter form makes possible the simple decomposition of the total ELI-D into directly additive, positive pELI-D contributions. In addition, it also corresponds to that representation which is directly related to the definition of chemically meaningful basins. Decompositions into canonical and localized orbitals for uncorrelated wavefunctions and natural orbitals from correlated wavefunctions have been discussed. Owing to the generality of the approach, similar decompositions can be made for systems with translation symmetry, for example, with respect to **k**-space-summed bands or Wannier functions.

It has been shown that this new technique of ELI-D decomposition provides additional insights into the ELI-D and ELF topologies from a one particle point of view. Differences in the electronic structures of two molecules, which can be understood in terms of classical orbital mixing concepts, can be directly related to their total ELI-D topology. The effect of using a correlated wavefunction (CAS level) with partial occupation of antibonding orbitals on the ELI-D topology of a sensible molecule has been shown for $F_2$. Interestingly, the ELI-D topology calculated from the "Kohn–Sham determinantal wavefunction" is closer to the CAS result than the one determined from the Hartree–Fock wavefunction. In all other cases considered here, the results from both single-determinantal methods are qualitatively the same. This suggests that the ELI-D calculated from the "Kohn-Sham determinantal wavefunction" should be considered to be at least on a similar level in terms of accuracy as the HF one.

  

To obtain a basic understanding of the formation of a certain total ELI-D topology from a collection of pELI-D contributions with different topologies, the general superposition mechanism has been discussed for several examples leading to the concealment of topological features of single pELI-D contributions in the total ELI-D distribution.

The structuring of the penultimate shell as a signature for the participation of its genuine orbitals in chemical bonding has been analyzed on the basis of the pELI-D orbital contributions for two transition-metal-containing molecules. Quantification of the spatial structuring of the total ELI-D by means of a newly defined structuring index $\varepsilon$ and analysis of the pELI-D orbital contributions to it lead to a refinement of the picture given in the literature. For the $Sc_2^{2+}$ molecule the structuring of the penultimate shell is caused not only by the true valence 3d states (60%), but through the semicore orbitals as well (40%). Surprisingly, along $r$ the 3d ($3\pi_u$ orbitals) pELI-D contributions monotonically cross their genuine (third shell) region and do not display an attractor there. For the $TiF_4$ molecule the observed titanium penultimate-shell structuring and its ligand-opposed pattern has been shown to be mainly caused by F–Ti bonding orbitals and to a lesser extent by closed-shell interactions of the F(2s)–Ti(3s,3p) type.

Finally, suitably localized orbitals and their pELI-D contributions have been shown to locally yield a picture closer to the final topology of the total ELI-D than those of single canonical orbitals. Compared with the chemical and physical information contained in localized orbitals, the ELI-D is the more general quantity. It is independent of the localization method as are the total electron density and the total energy. This gives rise to the question as to whether there is a possibility of constructing localized orbitals or functions using ELI-D topological information in the localization condition. Because a direct relationship between the ELI-D and electron localizability within the framework of event probabilities is known to exist,[3] this could give rise to really intrinsically localized orbitals or functions as a refined ingredient for the analysis of electronic interactions in molecules and solids.

## Appendix

**Relationship between the ELI-D and ELF**: To elucidate the connection between the ELI-D and ELF as defined by Becke and Edgecombe,[1] the Fermi hole curvature $g(\boldsymbol{r})$ for the case of a time-independent HF wavefunction has to be supplied. In the case of a time-independent approximate single-determinantal wavefunction, $g(\boldsymbol{r})$ simplifies[2,6] to Equation (12) with orbitals $\phi_i(\boldsymbol{r})$. At this level of theory the ELI-D from Equation (8) is given by Equation (13).

$$\begin{aligned} g(\boldsymbol{r}) &= \sum_{i<j}^{\mathrm{occ},\sigma} |\phi_i(\boldsymbol{r})\nabla\phi_j(\boldsymbol{r}) - \phi_j(\boldsymbol{r})\nabla\phi_i(\boldsymbol{r})|^2 \\ &= \rho_\sigma(\boldsymbol{r})\left(\sum_i^{\mathrm{occ},\sigma} |\nabla\phi_i(\boldsymbol{r})|^2 - \frac{1}{4}\frac{[\nabla\rho_\sigma(\boldsymbol{r})]}{\rho_\sigma(\boldsymbol{r})}\right) \end{aligned} \tag{12}$$

$$\begin{aligned} \Upsilon_{D,\mathrm{HF}}^{\sigma}(\boldsymbol{r}) &= \left[\frac{12\rho_\sigma(\boldsymbol{r})^{8/3}}{\rho_\sigma(\boldsymbol{r})\left(\sum_i^{\mathrm{occ},\sigma} |\nabla\rho_i(\boldsymbol{r})|^2 - \frac{1}{4}\frac{[\nabla\rho_\sigma(\boldsymbol{r})]^2}{\rho_\sigma(\boldsymbol{r})}\right)}\right]^{3/8} \\ &= \left[\frac{12\rho_\sigma(\boldsymbol{r})^{5/3}}{\sum_i^{\mathrm{occ},\sigma} |\nabla\rho_i(\boldsymbol{r})|^2 - \frac{1}{4}\frac{[\nabla\rho_\sigma(\boldsymbol{r})]^2}{\rho_\sigma(\boldsymbol{r})}}\right]^{3/8} \end{aligned} \tag{13}$$

The expression after the second identity provides a direct link to the kernel of the electron localization function (ELF) defined by Becke and Edgecombe[1] for a HF wavefunction. The ELF formula as defined by Becke and Edgecombe for the same-spin component of the wavefunction is built from a kernel $\chi^{\mathrm{ELF}}(\boldsymbol{r})$, which contains all the relevant information, and a mathematical scaling procedure applying a Lorentzian-type scaling, which serves to give the ELF function $\eta(\boldsymbol{r})$ desirable shape and values bound between 0 and 1 [Eq. (14)].

$$\eta(\boldsymbol{r}) = \frac{1}{1 + \left(\frac{D_\sigma(\boldsymbol{r})}{D_\sigma^0(\boldsymbol{r})}\right)^2} = \frac{1}{1 + [\chi^{\mathrm{ELF}}(\boldsymbol{r})]^2} \tag{14}$$

$$[\chi^{\mathrm{ELF}}(\boldsymbol{r})]^{-1} = \frac{2^{5/3}C_{\mathrm{F}}\rho_\sigma^{5/3}(\boldsymbol{r})}{\sum_i^{\mathrm{occ},\sigma} |\nabla\phi_i|^2 - \frac{1}{4}\frac{[\nabla\rho_\sigma(\boldsymbol{r})]^2}{\rho_\sigma(\boldsymbol{r})}} \tag{15}$$

Comparison of the ELF kernel [Eq. (15)] with the expression for the ELI-D in Equation (13) reveals that the numerical constant $2^{2/3}C_{\mathrm{F}}$ (the Fermi constant $C_{\mathrm{F}} = \frac{3}{10}(3\pi^2)^{2/3}$) appearing in the original definition of the ELF derived from the electron gas reference is not present in the ELI-D. Still, both quantities display the same topology. The fact that the ELI-D has a unique and simple physical meaning and that it is inherently defined for a fully correlated wavefunction as well are its decisive advantages. In contrast, $\chi^{\mathrm{ELF}}(\boldsymbol{r})$ is simply the ratio between two same-spin conditional pair probability density curvatures, namely $D_\sigma(\boldsymbol{r})$ of the actual system at point $\boldsymbol{r}$ and $D_\sigma^0(\boldsymbol{r})$ of the homogeneous electron gas with the same density as at point $\boldsymbol{r}$ of the actual system.

At this point it is important to recall Becke's intention of placing the ELF kernel into the denominator of his definition of the ELF:[1] the ELF kernel, interpreted as "a measure of electron localization", displays inverse behavior with respect to "electron localization". High values of $\chi^{\mathrm{ELF}}(\boldsymbol{r})$ are associated with low localizability and vice versa. Therefore, the ELF has been defined to show the topology of $[\chi^{\mathrm{ELF}}(\boldsymbol{r})]^{-1}$. Although it may be regarded as trivial and even as an arbitrary step at first glance, for the topological analysis of ELF it was an important step. Upon inverting the ELF kernel all critical points remain at their positions but their topological properties change: a local maximum (attractor) of $[\chi^{\mathrm{ELF}}(\boldsymbol{r})]^{-1}$ becomes a local minimum (repeller) of $\chi^{\mathrm{ELF}}(\boldsymbol{r})$ and vice versa. Therefore the basins of $\chi^{\mathrm{ELF}}(\boldsymbol{r})$ and $[\chi^{\mathrm{ELF}}(\boldsymbol{r})]^{-1}$ are completely different. From experience with topological analyzes of the ELF for many chemical systems it is clear that the basins of $[\chi^{\mathrm{ELF}}(\boldsymbol{r})]^{-1}$ have a chemical meaning, but those of $\chi^{\mathrm{ELF}}(\boldsymbol{r})$ do not. Within the framework of the ELI they directly correspond to the ELI-D and it is therefore this quantity that is analyzed throughout this contribution.

**Is an analogous charge decomposition of the ELF possible?** The relationship between the ELI-D at a time-independent HF level and the ELF is evident from a comparison of Equations (13) and (15). In contrast to the pair-restricted charge distribution $\Upsilon_D^\sigma(\boldsymbol{r})$, the decomposition of $\chi^{\mathrm{ELF}}(\boldsymbol{r})$ or $[\chi^{\mathrm{ELF}}(\boldsymbol{r})]^{-1}$ into separate orbital contributions is not uniquely fixed. Nevertheless, within the pseudopotential and effective core potential approach, the ELF for only the valence electrons was quite often calculated in the early ELF days, for example, by Savin et al.[25] As an approximate expression for the ELF in the valence region Equation (16) has been used.

$$[\chi^{\mathrm{ELF}}(\boldsymbol{r})]^{-1} \approx \frac{C_{\mathrm{F}}\left(\sum_i^{\mathrm{val.el.}} \rho_i(\boldsymbol{r})\right)^{5/3}}{\sum_i^{\mathrm{val.el.}} |\nabla\phi_i(\boldsymbol{r})|^2 - \frac{1}{4}\frac{[\nabla\sum_i^{\mathrm{val.el.}}\rho_i(\boldsymbol{r})]^2}{\sum_i^{\mathrm{val.el.}}\rho_i(\boldsymbol{r})}} = \frac{C_{\mathrm{F}}\left(\sum_i^{\mathrm{val.el.}} \rho_i(\boldsymbol{r})\right)^{5/3}}{\sum_i^{\mathrm{val.el.}} \frac{1}{4}\frac{[\nabla\rho_i(\boldsymbol{r})]^2}{\rho_i(\boldsymbol{r})} - \frac{1}{4}\frac{[\nabla\sum_i^{\mathrm{val.el.}}\rho_i(\boldsymbol{r})]^2}{\sum_i^{\mathrm{val.el.}}\rho_i(\boldsymbol{r})}} \tag{16}$$

  

The validity of this procedure in the sense of an approximation to the all-electron ELF in the valence region has been discussed in ref. [26]. According to that study, a good approximate valence-only ELF can be expected only when both the valence and the core orbitals do not have large contributions in the same regions of space. In spite of this, the same scheme was later utilized by Santos et al. in order to extract selected π orbital contributions.[27] As the σ and π contributions are large in the same regions of space it is clear that such a procedure is in fact no longer related to the ELF. It is evident that separate σ and π contributions defined in this way are not additive even for the kernel of the ELF. Furthermore, single orbital contributions of, for example, the π orbital of $C_2H_4$ cannot be analyzed with that decomposition because the denominator of the inverse kernel is equal to zero in this case (cf. Equation (16) after the second identity). In contrast, complete orbital decomposition of ELI-D for $C_2H_4$ is possible and it is explicitly shown in the examples above. Furthermore, from Equation (11) the calculation of the valence electrons' contributions to the total ELI-D is physically transparent: it is simply the sum of the orbital densities of all the valence electrons times the scaled pair volume function calculated from all electrons. This is shown and used in the examples above for the argon atom and for molecules of $N_2$ and $F_2$.

To achieve an orbital decomposition of the inverse ELF kernel $[\chi^{\mathrm{ELF}}(\boldsymbol{r})]^{-1}$ similar to Equation (11) with additive contributions would involve the application of Equation (17) which involves splitting the homogenous electron gas expression in the numerator into two density-dependent parts only one of which is then decomposed into orbital contributions, whereas the term in the denominator, which is interpreted to contain the localization information of the system,[1] is not decomposed at all. Within the framework of the ELF, such a procedure is hardly justified and it is no surprise that this orbital decomposition scheme has not even been thought of. This clearly demonstrates the completely different approach of the pair-restricted charge distribution ELI-D, which is physically meaningful and transparent. The orbital decomposition given by Equation (11) is only justified within the restricted populations approach, giving rise to the same-spin pair-restricted charge population. Decomposition of the ELF according to Equation (17) would correspond to a reinterpretation of Becke's ELF formula in the sense of the pair-restricted charge (i.e., ELI-D), which would still not be consistent, however, because the Fermi constant $C_F$ has no justification there.

$$[\chi^{\mathrm{ELF}}(\boldsymbol{r})]^{-1} = \frac{C_F \rho_\sigma^{5/3}(\boldsymbol{r})}{\sum_i^{\mathrm{occ},\sigma} |\nabla\phi_i(\boldsymbol{r})|^2 - \frac{1}{4}\frac{[\nabla\rho_\sigma(\boldsymbol{r})]^2}{\rho_\sigma(\boldsymbol{r})}} = \sum_i^{\mathrm{occ},\sigma} \rho_i(\boldsymbol{r}) \frac{C_F \rho_\sigma^{2/3}(\boldsymbol{r})}{\sum_i^{\mathrm{occ},\sigma} |\nabla\phi_i(\boldsymbol{r})|^2 - \frac{1}{4}\frac{[\nabla\rho_\sigma(\boldsymbol{r})]^2}{\rho_\sigma(\boldsymbol{r})}} \tag{17}$$

Recently, a reinterpretation of Becke's ELF, valid also for the fully correlated wavefunction, was claimed by Matito et al.[28] The kernel of this function is the so-called spin-pair composition function $c_\pi$, which is defined by Silvi[29] as the scaled ratio $D_s(\boldsymbol{r})$ [Eq. (18)] between the parallel spin-pair concentration $\bar{N}_\parallel(\boldsymbol{r})$ with a finite arbitrary sampling volume around the reference point $\boldsymbol{r}$ given by Equation (19) and the "pair concentration of a single pair" $\frac{1}{2}\bar{N}(\boldsymbol{r})^2$, which is obtained from the "number of antiparallel pairs in the limit of non-interacting electrons in a singlet state"[29] [Eq. (20)].

$$c_\pi(\boldsymbol{r}) = D_s(\boldsymbol{r})\bar{N}(\boldsymbol{r})^{-2/3} = 2\frac{\bar{N}_\parallel(\boldsymbol{r})}{\bar{N}(\boldsymbol{r})^2}\bar{N}(\boldsymbol{r})^{-2/3} = 2\frac{\bar{N}_\parallel(\boldsymbol{r})}{\bar{N}(\boldsymbol{r})^{8/3}} \tag{18}$$

$$\bar{N}_\parallel(\boldsymbol{r}) = \int_V\int_V \rho_2^{\alpha\alpha}(\boldsymbol{r}_1,\boldsymbol{r}_2)\mathrm{d}\boldsymbol{r}_1\mathrm{d}\boldsymbol{r}_2 + \int_V\int_V \rho_2^{\beta\beta}(\boldsymbol{r}_1,\boldsymbol{r}_2)\mathrm{d}\boldsymbol{r}_1\mathrm{d}\boldsymbol{r}_2 \tag{19}$$

$$\bar{N}_\perp^0(\boldsymbol{r}) = \frac{1}{2}\int_V \rho(\boldsymbol{r}_1)\mathrm{d}\boldsymbol{r}_1 \int_V \rho(\boldsymbol{r}_2)\mathrm{d}\boldsymbol{r}_2 = \frac{1}{2}\bar{N}(\boldsymbol{r})^2 \tag{20}$$

Taylor expansion of $\rho_s^{\sigma\sigma}(\boldsymbol{r}_1,\boldsymbol{r}_2)$ in Equation (19) for $\bar{N}_\parallel(\boldsymbol{r})$ and by assuming Equation (21), which is used to eliminate the dependence of $\bar{N}_\parallel(\boldsymbol{r})$ on the arbitrary sampling volume $V$, finally yields Equation (22).

$$\bar{N}(\boldsymbol{r}) \approx \rho(\boldsymbol{r})V \tag{21}$$

$$c_\pi(\boldsymbol{r}) = \frac{\nabla_s^2\rho_2^{\alpha\alpha}(r,r+s)|_{s=0} + \nabla_s^2\rho_2^{\beta\beta}(r,r+s)|_{s=0}}{3\rho(\boldsymbol{r})^{8/3}} \tag{22}$$

Equation (22) was later put, in analogy with the ELF, into the Lorentzian form $1/[1+c_\pi(\boldsymbol{r})^2]$, including a scaling with the Fermi constant $C_F$.[28]

From Equations (18) and (22) it is evident that an orbital decomposition of the inverse kernel $[c_\pi(\boldsymbol{r})]^{-1}$ in a similar way to the ELI-D [Eq. (11)] is not possible for the same reason as for the ELF: conceptually, there is no separate quantity $\rho(\boldsymbol{r})$ that can be factorized out of the numerator of $[c_\pi(\boldsymbol{r})]^{-1}$ and be treated differently from the remaining $\rho(\boldsymbol{r})^{5/3}$ term.

## Acknowledgements

We thank Prof. Dr. G. Miller for critical reading of the manuscript. Funding by the Deutsche Forschungsgemeinschaft (SPP1166) is acknowledged.

[1] A. D. Becke, K. E. Edgecombe, *J. Chem. Phys.* **1990**, *92*, 5397–5403.
[2] M. Kohout, *Int. J. Quantum Chem.* **2004**, *97*, 651–658.
[3] M. Kohout, F. R. Wagner, Yu. Grin, unpublished results.
[4] M. Kohout, F. R. Wagner, Yu. Grin, *Int. J. Quantum Chem.* **2006**, *106*, 1499–1507.
[5] M. Kohout, *Faraday Discuss.* **2007**, *135*, 43–54.
[6] M. Kohout, K. Pernal, F. R. Wagner, Yu. Grin, *Theor. Chem. Acc.* **2004**, *112*, 453–459.
[7] J. F. Dobson, *J. Chem. Phys.* **1991**, *94*, 4328–4333.
[8] R. F. W. Bader, Atoms in Molecules—A Quantum Theory, Clarendon Press, Oxford, **1995**.
[9] E. J. Baerends, O. V. Gritsenko, *J. Phys. Chem. A* **1997**, *101*, 5383–5403.
[10] MOLPRO, version 2006.1, a package of ab initio programs, H.-J. Werner, P. J. Knowles, R. Lindh, F. R. Manby, M. Schütz, P. Celani, T. Korona, G. Rauhut, R. D. Amos, A. Bernhardsson, A. Berning, D. L. Cooper, M. J. O. Deegan, A. J. Dobbyn, F. Eckert, C. Hampel, G. Hetzer, A. W. Lloyd, S. J. McNicholas, W. Meyer, M. E. Mura, A. Nicklass, P. Palmieri, R. Pitzer, U. Schumann, H. Stoll, A. J. Stone, R. Tarroni, T. Thorsteinsson, Cardiff (UK), **2006** (http://www.molpro.net).
[11] G. Karlström, R. Lindh, P.-Å. Malmqvist, B. O. Roos, U. Ryde, V. Veryazov, P.-O. Widmark, M. Cossi, B. Schimmel-Pfennig, P. Neogrady, L. Seijo, *Comput. Mater. Sci.*, **2003**, *28*, 222–239 (MOLCAS, version 6.4).
[12] ADF2005.01, E. J. Baerends, J. Autschbach, A. Bérces, C. Bo, P. M. Boerrigter, L. Cavallo, D. P. Chong, L. Deng, R. M. Dickson, D. E. Ellis, M. van Faassen, L. Fan, T. H. Fischer, C. Fonseca Guerra, S. J. A. van Gisbergen, J. A. Groeneveld, O. V. Gritsenko, M. Grüning, F. E. Harris, P. van den Hoek, H. Jacobsen, L. Jensen, G. van Kessel, F. Kootstra, E. van Lenthe, D. A. McCormack, A. Michalak, V. P. Osinga, S. Patchkovskii, P. H. T. Philipsen, D. Post, C. C. Pye, W. Ravenek, P. Ros, P. R. T. Schipper, G. Schreckenbach, J. G. Snijders, M. Solà, M. Swart, D. Swerhone, G. te Velde, P. Vernooijs, L. Versluis, O. Visser, F. Wang, E. van Wezenbeek, G. Wiesenekker, S. K. Wolff, T. K. Woo, A. L. Yakovlev, T. Ziegler, SCM, Theoretical Chemistry, Vrije Universiteit, Amsterdam, **2005** (http://www.scm.com).
[13] A. D. Becke, *Phys. Rev. A* **1988**, *38*, 3098–3100.
[14] C. Lee, W. Yang, R. G. Parr, *Phys. Rev. B* **1988**, *37*, 785–789.
[15] Program DGrid, version 4.0, M. Kohout, Max-Planck-Institut für Chemische Physik fester Stoffe, Dresden, **2006**.
[16] Y. Tal, R. F. W. Bader, *Int. J. Quantum Chem., Quantum Chem. Symp.* **1978**, *12*, 153–168.
[17] M. Kohout, A. Savin, *Int. J. Quantum Chem.* **1996**, *60*, 875–882.
[18] M. Kohout, unpublished results.
[19] J. M. Foster, S. F. Boys, *Rev. Mod. Phys.* **1960**, *32*, 300–302.

  

[20] C. Edmiston, K. Ruedenberg, *Rev. Mod. Phys.* **1963**, *35*, 457–465.
[21] a) W. England, *Int. J. Quantum Chem.* **1971**, *5*, 683–697; b) P. Scheurer, W. H. E. Schwarz, *Int. J. Quantum Chem.* **2000**, *76*, 420–427.
[22] M. Kohout, F. R. Wagner, Yu. Grin, *Theor. Chem. Acc.* **2002**, *108*, 150–156.
[23] R. J. Gillespie, S. Noury, J. Pilme, B. Silvi, *Inorg. Chem.* **2004**, *43*, 3248–3256.
[24] K. Pierloot, *Mol. Phys.* **2003**, *101*, 2083–2094.
[25] A. Savin, A. D. Becke, J. Flad, R. Nesper, H. Preuss, H. G. von Schnering, *Angew. Chem.* **1991**, *103*, 421–424; *Angew. Chem. Int. Ed. Engl.* **1991**, *30*, 409–412.
[26] M. Kohout, A. Savin, *J. Comput. Chem.* **1997**, *18*, 1431–1439.
[27] J. C. Santos, W. Tiznado, R. Contreras, P. Fuentealba, *J. Chem. Phys.* **2004**, *120*, 1670–1673.
[28] E. Matito, B. Silvi, M. Duran, M. Sola, *J. Chem. Phys.* **2006**, *125*, 024301-1.
[29] B. Silvi, *J. Phys. Chem. A* **2003**, *107*, 3081–3085.

Received: January 4, 2007
Published online: April 25, 2007

  